J. Fluid Mech. (1994), *vol.* 261, *pp.* 135–168

Drop formation during coating of vertical fibres

By SERAFIM KALLIADASIS AND HSUEH-CHIA CHANG
Department of Chemical Engineering, University of Notre Dame, Notre Dame, IN 46556, USA

(Received 21 October 1992 and in revised form 23 August 1993)

When the coating film around a vertical fibre exceeds a critical thickness h_c, the interfacial disturbances triggered by Rayleigh instability can undergo accelerated growth such that localized drops much larger in dimension than the film thickness appear. We associate the initial period of this strongly nonlinear drop formation phenomenon with a self-similar intermediate asymptotic blow-up solution to the long-wave evolution equation which describes how static capillary forces drain fluid into the drop. Below h_c, we show that strongly nonlinear coupling between the mean flow and axial curvature produces a finite-amplitude solitary wave solution which prevents local finite-time blow up and hence disallows further growth into drops. We thus estimate h_c by determining the existence of solitary wave solutions. This is accomplished by a matched asymptotic analysis which joins the capillary outer region of a large solitary wave to the thin-film inner region. Our estimate of $h_c = 1.68R^3H^{-2}$, where R is the fibre radius and H is the capillary length $H = (\sigma/\rho g)^{\frac{1}{2}}$, is favourably compared to experimental data.

1. Introduction

An important phenomenon in the coating of wire or fibres is the break up of the thin annular film into drops (see figure 1). The physical mechanism that drives this drop formation process is the classical Rayleigh instability for cylindrical interfaces. The same capillary instability, induced initially by azimuthal curvature variation in the axial direction, also causes liquid jet break up, snap-off of lubricated air threads (Aul & Olbricht 1990) or break up of the annular film into lobes in capillaries (Hammond 1983; Frenkel *et al.* 1987). It is an azimuthally symmetric instability with a characteristic axial wavelength of

$$\lambda_c = 2\pi\sqrt{2}R, \tag{1}$$

where R is the radius of the cylindrical interface.

In a recent study of the drop formation process in coating flow by Quéré (1990), a unique nonlinear saturation phenomenon is observed. If the coating film is below a critical film thickness h_c, which is found to scale as R^3, the Rayleigh instability seems to be saturated by nonlinear effects associated with the mean flow such that the disturbances do not grow unarrested as in the case of jet and annular film break up, and air thread snap-off. Instead, small-amplitude interfacial waves were observed. It is only beyond h_c that one observes the unbounded growth into drops which have a characteristic height as large as the wavelength λ_c.

A simple scaling argument by Frenkel (1992) offers some insight into how this mean-flow nonlinear saturation process occurs for coating flow. Using the usual long-wave expansion, and assuming creeping flow conditions, thin liquid films and strong

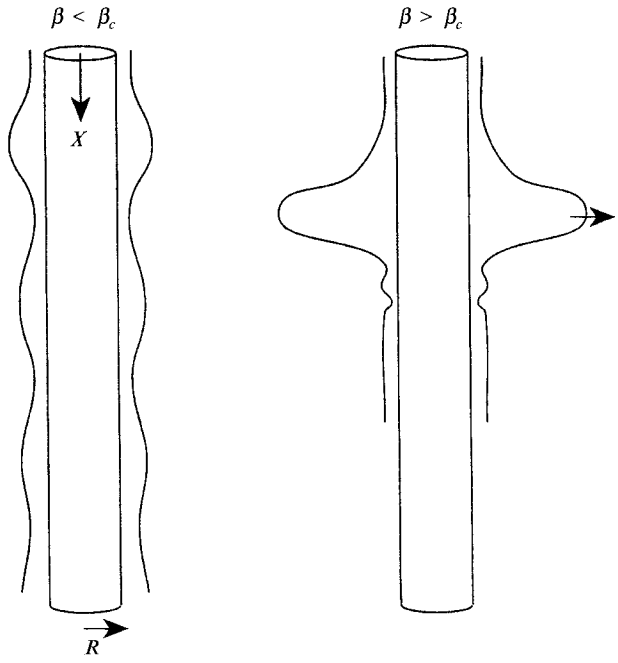

FIGURE 1. Schematic of saturated interfacial waves on a fibre with a thin film ($\beta < \beta_c$) and the formation of large drops with a thick film ($\beta > \beta_c$).

capillary effects ($W \gg 1$), he has derived the following evolution equation for the axisymmetric interface around a fibre,

$$\frac{\partial h}{\partial t}+\frac{\partial}{\partial x}\left(\frac{2}{3}h^3\right)+\epsilon\frac{\partial}{\partial x}\left[\frac{2}{3}\frac{W}{a^2}h^3h_x+\frac{2}{3}We^2h^3h_{xxx}\right]=0 \tag{2}$$

where h has been scaled with respect to the spatially averaged thickness h_0, the axial coordinate x by λ_c and t by the convective timescale an interfacial particle transverses one wavelength λ_c, $\tau_c = (2\lambda_c \nu/gh_0^2)$. The other parameters are the film parameter $\epsilon = h_0/\lambda_c \ll 1$ which is also the expansion parameter, the Weber number

$$W = \sigma/\rho g h_0^2 \sim O(\epsilon^{-2})$$

and the dimensionless fibre radius $a = R/h_0 \sim O(\epsilon^{-1})$. In (2), the second term is the convective term due to mean flow while the third and fourth terms correspond to azimuthal and axial curvatures respectively. The azimuthal curvature term is destabilizing while the axial curvature term is stabilizing as one can easily decipher from a weakly nonlinear expansion of (2)

$$h \sim 1+\hat{h}, \tag{3}$$

where $\hat{h} \sim O(\epsilon)$,

$$\frac{\partial \hat{h}}{\partial t}+2\frac{\partial \hat{h}}{\partial x}+4\hat{h}\frac{\partial \hat{h}}{\partial x}+\frac{2}{3}W\left[\left(\frac{\epsilon}{a^2}\right)\frac{\partial^2 \hat{h}}{\partial x^2}+\epsilon^3\frac{\partial^4 \hat{h}}{\partial x^4}\right]=0, \tag{4}$$

which can be rescaled into the Kuramoto–Sivashinsky equation in (6). Cheng & Chang (1992) have shown that the prediction from the linearized version of (4) (or (2)) for infinitesimal waves near inception, a critical wavelength of λ_c and a phase speed twice the interfacial velocity $2(gh_0^2/2\nu)$, are in good agreement with the inception data for

small cylinders with dominant capillary effects and with the numerical result from the linearized equation of motion at low Reynolds number and high surface tension. Saturation of this linear growth must then involve a balance of the nonlinear convective term $\hat{h}(\partial\hat{h}/\partial x)$ with the two curvature terms. Note that, in both (2) and (4), this convective term contains an odd derivative which breaks the $x \to -x$ symmetry. Physically, this causes an asymmetric steepening of the wave front in the x-direction as the wave grows, since higher interfacial positions travel faster. This mechanism increases the axial curvature and hence balances the destabilizing azimuthal curvature term. The same mechanism is also in play in (2) but it is then strongly nonlinear. One can render this balance of the asymmetric convective and symmetric curvature terms more precise by rescaling time and spatial coordinates,

$$x \to W^{-\frac{1}{3}}\epsilon^{-1}x, \tag{5a}$$

$$t \to \tfrac{2}{3}W^{-\frac{1}{3}}\epsilon^{-1}t, \tag{5b}$$

to yield the weakly nonlinear version

$$\frac{\partial\hat{h}}{\partial t}+3\frac{\partial\hat{h}}{\partial x}+6\hat{h}\frac{\partial\hat{h}}{\partial x}+\beta\hat{h}_{xx}+\hat{h}_{xxxx}=0, \tag{6}$$

and the fully nonlinear equation

$$\frac{\partial h}{\partial t}+[h^3+\beta h^3 h_x+h^3 h_{xxx}]_x=0, \tag{7}$$

where

$$\beta = W^{\frac{2}{3}}/a^2. \tag{8}$$

The strongly nonlinear equation (7) reduces to Hammond's equation (Hammond 1983) for annular films in a capillary without the mean flow term $(h^3)_x$. The weakly nonlinear version (6) becomes the Kuramoto–Sivashinsky equation after a moving-coordinate transformation to remove the linear convective term $3(\partial\hat{h}/\partial x)$. The factor of 3 results from the transformation (5) which implies that an infinitesimally small wave travels at a phase speed three times the mean velocity or twice the interfacial velocity.

For nonlinear saturation by mean flow to be effective, the mean-flow, axial and azimuthal curvature terms in (6) and (7) must balance. Consequently, β should be of order unity which yields the scaling law observed by Quéré (1990) and first explained by Frenkel (1992),

$$h_c \sim R^3 H^{-2}, \tag{9}$$

where $H = (\sigma/\rho g)^{\frac{1}{2}}$ is the capillary lengthscale. Since this nonlinear saturation mechanism is induced by the mean flow due to viscous gravitational drainage, it is absent in horizontal fibres, inviscid liquid jets and annular films in capillaries without primary flow. In the last case, the annular film either breaks up into symmetric lobes with each lobe described by (Hammond 1983)

$$h = A(1+\cos\beta^{\frac{1}{2}}x), \tag{10}$$

which corresponds to a long-wave expansion of the unduloid solution family to the Laplace–Young equation. The interface simply evolves through each member of an unduloid family parameterized by A. The above argument then suggests that if viscous flow is also induced in these systems, the above phenomenon can be prevented. This has been qualitatively verified by the experiment of Aul & Olbricht (1990) and the scaling arguments of Frenkel *et al.* (1987) for annular films in a capillary. It is also

related to Russo & Steen's observation (1989) that viscous shear can stabilize the Rayleigh instability of a liquid cylinder.

Several assumptions have been invoked in the derivation of (7). We shall examine some of them next. An important omitted effect is inertia which is the dominant destabilizing mechanism for falling film on a plane or a large cylinder where Rayleigh azimuthal instability is weak. It is then pertinent to determine how thin the fibre should be before inertia can be safely neglected. As derived in detail by Lin (1974), the leading-order streamwise velocity u_0 in any interfacial lubrication flow falling under gravity low Reynolds number and long waves scales as $\rho g h_0^2/\mu$. The next order correction u_1 in velocity in the expansion in the film parameter ϵ then contains an inhomogeneous part owing to the contribution of the leading-order term through the nonlinear inertia term. This inhomogeneous term is of the order $\rho(\rho g h_0^2/\mu)^2/l$ where l is the characteristic wavelength ($\epsilon = h_0/l$ here). The velocity correction due to inertia is then of order $(g^2 h_0^6/l\nu^3)$. In the final evolution equation for h, it is this inertia-induced second-order velocity that provides the destabilizing growth term $(\partial/\partial x)\int_0^h u_1 \, dy$ which yields a film growth rate of order $(h_0^7 g^2/l^2\nu^3)$. For saturated waves in high-surface-tension fluid, this inertia instability is arrested by the same axial curvature term in (2) which scales as $(\sigma h_0^4/\mu l^4)$. Balance of these two terms then yields a characteristic wavelength for inertia instability in falling films

$$l = H\nu/(g h_0^3)^{\frac{1}{2}}, \tag{11}$$

and a characteristic film growth rate of

$$r_I = (h_0^{10} g^3/H^2\nu^5). \tag{12}$$

For Rayleigh-instability-dominated films on thin fibres, the characteristic wavelength is $\lambda_c \sim R$ in (1) and the Rayleigh growth rate is

$$r_R = \frac{\sigma h_0^4}{\mu R^4}. \tag{13}$$

Balancing r_I and r_R, one obtains a critical R^* below which ($R \ll R^*$) inertia can be neglected

$$R^* = \left(\frac{H\nu}{h_0^{\frac{3}{2}} g^{\frac{1}{2}}}\right) = l, \tag{14}$$

which is simply a balance of the capillary lengthscale $\lambda_c \sim R$ with the inertia dominated lengthscale l. In a continuously falling film with a constant flow rate Q supplied from the top $h_0 = (3\nu Q/g)^{\frac{1}{3}}$. If one uses a Reynolds number Re to measure the flow rate, $Re = Q/\nu$, then $h_0 = (3Re\nu^2/g)^{\frac{1}{3}}$ and $R^* = l = (H/3^{\frac{1}{2}})Re^{-\frac{1}{2}}$. For water, $H \sim 2.7$ mm and the inertia effect can be important for moderate flow rates ($Re \sim O(1)$) if the fibre radius is of the order of the capillary length. One then requires $R \ll H$ for inertia to be negligible. In most coating flows, however, the film is applied by running the fibre or plane through a pool of liquid in a 'drag-out' (Wilson 1982) or 'drag-in' process (Wilson & Jones 1983). For the drag-out process, the film thickness scales as $RCa^{\frac{2}{3}}$ owing to a balance of viscous and capillary effects as in the Bretherton problem (Bretherton 1961). The scaling for coating film in the drag-in process is not known but it is typically very thin because of the possibility of air entrainment if the dragging speed U is too large. For the drag-out process, the critical R^* of (14) becomes

$$R^* \sim \left(\frac{H\nu}{Ca\, g^{\frac{1}{2}}}\right)^{\frac{2}{5}} = R_0\, Ca^{-\frac{2}{5}}, \tag{15}$$

where $Ca = \mu U/\sigma$ is the capillary number corresponding to the dimensionless drag out speed. For Quéré's experiment with silicone oil $H = 1.5$ mm and $\nu = 500$ mm^2 s^{-1}, $R_0 = (H\nu/g^{\frac{1}{2}})^{\frac{2}{5}} \sim 0.23$ cm while Ca is typically much less than unity ($\sim 10^{-2}$). For water, R_0 is 0.02 cm. Since σ/μ is as high as 10^4 cm/s for water, most industrial processes operate at $Ca \ll 1$ and any fibre coating process with fibres smaller than 0.5 cm in diameter can safely eliminate inertia as a cause for drop formation. Nevertheless, there can be a difference in the interfacial instabilities of continuous falling films and coating films in a drag-out process depending on the fibre radius. Because the film is extremely thin in the latter owing to a balance of capillary and viscous forces which yields the $Ca^{\frac{2}{3}}$ scaling for the film height, inertia effect is negligible compared to the azimuthal capillary effect.

Another assumption that should be scrutinized is the variation in time of the instantaneous average thickness h_0. In fibres coated by the drag-out process, which was used by Quéré, h_0 will decrease in time as the film drains. Since we will omit this dynamics in our quasi-steady formulation, the thinning rate of the film must be slow compared to the Rayleigh capillary growth rate r_R in (13). The characteristic timescale for film growth due to the Rayleigh instability is

$$\tau_R = h_0/r_R = (\mu R^4/\sigma h_0^3), \tag{16}$$

while the characteristic velocity for thinning is $(gh_0^2/3\nu)$ and hence the characteristic time for the thinning of the film is

$$\tau_T = 2\pi R h_0/(gh_0^3/3\nu), \tag{17}$$

which is consistent with the classical Reynolds lubrication thinning rate that scales as $\tau^{\frac{1}{2}}$. Consequently, after inserting (9) for drop formation conditions,

$$(\tau_R/\tau_T) \sim 1/6\pi \ll 1 \tag{18}$$

which justifies the quasi-steady approximation. Actually, the Rayleigh growth rate in (13) and (16) are underestimated because of the small-amplitude estimates. As we shall show, the nonlinear evolution rate of the drops is far larger than the estimates in (13) and hence the quasi-steady approximation is even better than that indicated by (18). In Quéré's study, a typical experiment requires on the order of one day to drain which is consistent with our estimate τ_T in (17) for a typical fibre radius of $R = 0.15$ mm under drop formation conditions of (9) but drops form in a matter of seconds or minutes while our estimate τ_R yields about 1 h for fibres of the same radius after using (9) in (16). This also suggests an underestimate of the drop formation rate.

Although the above scaling arguments provide the correct scaling for h_c in (9), a quantitative estimate of the coefficient in front of the expression, like the celebrated Bretherton constant in $h_0 \sim 1.337\, RCa^{\frac{2}{3}}$ (Bretherton 1961), requires a much more detailed analysis. Like break up of jets and annular films and snap-off of lubricated air threads in capillaries, a drop formation involves growth of the long wave length interfacial disturbances into extremely large structures. For thin vertical fibres with $R \ll H$, these drops have characteristic heights and lengths of the order R as compared to the small-amplitude disturbances with heights much smaller than R when drops do not form (see figure 1). The latter saturated disturbances are always present. When R is larger and approaches H, the drops will feel the effect of gravity as they grow and they will eventually resemble falling pendant drops. However, even in this case, the drops must first evolve through a stage when gravity is still unimportant but the drop height is already the same order as the wavelength. It is at this stage in both cases that

the aspect ratio of the drop first becomes incompatible with the lubrication approximation that leads to the evolution equation (7). This then suggests that drop formation in both cases corresponds to unbounded solutions of (7). That is, if one integrates (7) under conditions that drops form, an initially small disturbance will grow without bound as a localized structure, possibly in finite time. Localized blow-up behaviour has been noticed in numerical studies of two-dimensional falling films on inclined planes (Pumir *et al.* 1983; Rosenau, Oron & Hyman 1992). However, drop formations are typically not observed as viscous falling films on planes or large cylinders. These waves tend to have small amplitudes and develop transverse variations (fingers, etc.), instead of forming drops. As a result, two-dimensional blow-up solutions are treated as mathematical curiosities for planar or near-planar films. It is quite likely that introduction of capillary-driven transverse variation for the planar film will relax this numerical blow-up phenomenon (Schwartz 1989). The situation is quite different for small-radius annular or cylindrical films, however. Accelerated break ups of such interfaces are commonly observed in the systems described earlier (jets, air threads in capillaries and fibre coating) and they all occur while retaining axisymmetry provided the radius is small enough. The extreme stability of non-axisymmetric disturbances of annular and cylindrical falling films has been studied by Shlang & Sivashinsky (1982) who showed that non-axisymmetric disturbances are only linearly stable if

$$R < \left(\frac{5}{2}\right)^{\frac{1}{2}} \frac{Hv}{g^{\frac{1}{2}}h_0^{\frac{3}{2}}}. \tag{19}$$

For continuously falling films with $h_0 = (3Re\,\nu^2/g)^{\frac{1}{3}}$, this yields

$$R < \left(\frac{5}{6}\right)^{\frac{1}{2}} H\,Re^{-\frac{1}{2}}, \tag{20}$$

which again requires the fibre radius to be small relative to the capillary length. The condition is less stringent, however, for the drag-out process with $h_0 \sim RCa^{\frac{2}{3}}$,

$$R < R^*, \tag{21}$$

where R^* is given by (15). Since R^* is extremely large for most drag-out processes, any fibre smaller than 0.5 cm can ignore non-axisymmetric disturbances as well as inertia. Consequently, the growing axisymmetric disturbances of a thin annular/cylindrical film cannot transfer its energy to non-axisymmetric disturbances as waves on a plane ($R \to \infty$) do and can hence blow up while retaining its axisymmetry if they are not arrested by mean flow effects. Localized blow-up solutions of (2) are hence quite physical and are related to the drop formation process. In many finite-domain models, however, the finite amount of available liquid does not permit the blow-up structure to truly approach infinity in height. As a result, the blow-up solution is an intermediate asymptotic behaviour in time which is preceded by linear inception of the Rayleigh mechanism and followed by a slower drainage mechanism as the film thins. A blow-up behaviour that goes to completion in finite time can be achieved with more difficult and artificial boundary conditions that allow an infinite amount of liquid to develop within the domain in finite time. Nevertheless, even for domains with finite amount of available liquid we shall demonstrate both numerically and analytically that blow-up like accelerated growth occurs for a prolonged interval when β exceeds a critical value β_c such that the final structure height is dramatically higher for $\beta > \beta_c$. The determined β_c is in excellent agreement with Quéré's data for drop formation. It should also be

mentioned that the solution to the Kuramoto–Sivashinsky equation (6) can be shown to be always bounded. However, examination of the solution shows that the bounded deviation height $\hat{h}(x,t)$ often takes on values in excess of unity which violates the weakly nonlinear approximation that leads to (6). This then points out that finite-time blow up is a strongly nonlinear phenomenon that escapes the quadratic weakly nonlinear description of mean-flow interaction offered by (6). It also emphasizes that the Kuramoto–Sivashinsky equation is only appropriate for saturated small-amplitude waves whose amplitude is much smaller than the film thickness. It is not even appropriate for saturated waves with amplitudes as large as the film thickness. We shall hence abandon (6) in favour of the strongly nonlinear evolution equation (7) in our analysis although (6) clearly provides the correct scaling argument for mean-flow saturation.

In §2, we present a numerical study of (7) which demonstrates that intermediate asymptotic blow up persists for a long time for β beyond a critical value β_c. Local structures which resemble static drops described by (10) grow unhindered until the long-wavelength approximation becomes invalid or until the growth is limited by the supply of liquid through a thin constriction at a 'dimple'. Below β_c, the interfacial disturbances tend to develop into identical local structures (coherent structures) with saturated amplitudes which translate laterally. Although there is no growth in the amplitude, these coherent structures can interact laterally such that the large-time asymptotic state remains time-dependent although there is no blow up. In §3, we study the spatially localized blow-up solution analytically and show that it is an approximate self-similar solution to (7) whose normalized structure approaches the static solution described by (10). We also show that the coherent structures correspond to another self-similar solution, the solitary-wave solution. We argue that a family of solutions generated by the solitary waves dominates the dynamics such that all initial conditions approach this family of solutions locally instead of the blow-up solution. Growth into large drops is hence impossible. The intermediate blow-up behaviour is approached by some wave crests, however, when this solitary-wave solution does not exist. Spatially localized, finite-time blow up then occurs until it is arrested by the formation of a very thin dimple constriction in front of the blow-up structure. We hence focus our analysis on analytical and numerical construction of the solitary-wave solution in §4. It is shown that for $\beta > \beta_c = 1.41$, the mean flow effect becomes insufficient to allow solitary waves to exist. This result is in excellent agreement with Quéré's data for drop formation and without our numerical results for finite-time blow up. A conclusion is offered in §5.

During the course of this work, Kerchman & Frenkel (1993) have observed a specific mechanism for drop formation from their numerical experiments. They observed that drop formation seems to be triggered when two waves coalesce successively and inelastically and it does not happen if waves repel each other. We shall show numerical evidence that wave growth can also occur through drainage from the substrate film or from a smaller adjacent wave. In any case, all growth mechanisms seem to follow the blow-up solution initially. Hence, when blow up is suppressed by the solitary waves, growth towards drop formation is impossible by any mechanism. There is probably a link between repulsive wave (coherent structure) interaction and the blow-up behaviour but the connection is not clear. If one models the coherent structures by the solitary waves, as we have done in the falling film problem (Chang, Demekhin & Kopelevich 1993*b*), repulsive wave interaction definitely cannot occur if there are no solitary waves, coalescence will probably appear instead. A more specific analysis in this direction will be presented in a subsequent paper.

2. Numerical study

An extensive numerical study of (7) has been carried out using an implicit and quasi-linear Crank–Nicholson scheme. We impose periodic boundary conditions over a finite domain L that is much longer than the Rayleigh wavelength ($\lambda_c \sim 2^{\frac{3}{2}}\pi\beta^{\frac{1}{2}}$ in the dimensionless coordinate x). For $L = 50$, the space and time steps are lower than $\Delta x = \Delta t = 0.05$ to ensure numerical stability which is checked by examining the constancy of $\int_0^L h(x,t)\,dx$ in time guaranteed by the mass conservation property of (7). It should be noted that, with periodic boundary conditions, this mass conservation property of (7) can never allow blow up in finite time since the latter implies that the total mass within the localized blow-up structure grows explosively to infinity in finite time. As such, our blow-up solution is a self-similar intermediate asymptotics in time for periodic boundary conditions and the construction in the next section is an analysis valid only for a localized position and for a certain intermediate interval in time. It should also be noted that a simple analysis of our self-similar blow-up solution yields the result that the volume within the structure will reach infinity in finite time – a clear violation of the mass conservation property with finite periodic boundary conditions. In contrast, the blow-up solutions of Pumir *et al.* (1983) for falling films on a plane and of Rosenau *et al.* (1992) tend to approach zero volume at they grow since their width shrinks faster than their amplitude growth. Our blow-up solution reaches a constant width and hence its volume scales as the amplitude. We will show that a 'dimple' constriction will eventually develop in front of our structure as the film thins and arrest the blow-up behaviour as it throttles the drainage of fluid into the structure. This small dimple is not considered in our leading-order construction of the blow-up solution. Even though our blow-up growth is a transient phenomenon, this explosive strongly nonlinear mechanism nevertheless greatly accelerates the growth of a particular wave crest and, in fact, permits amplitude growth to form drops. Its suppression therefore suggests that amplitude growth to form drops is impossible. We also show numerical evidence that the blow up will go to completion in finite time if there is an infinity of available liquid.

Using the same single-harmonic initial condition $h(x,0) = 1 - 0.1\cos(2\pi x/L)$, we carried out a series of runs for various β values between 0.1 and 2.0. For $\beta < 1.2$, the small-amplitude initial condition quickly evolves into a modulated periodic wavetrain with the wavelength close to λ_c according to linear stability theory. Some slight adjustment occurs when L is not an integer multiple of λ_c but the number of wave crests after the linear inception region is always equal to the integer immediately above or below L/λ_c. The inception region spans a timescale of order $-4lnh_i/\beta^2$ where h_i is the initial amplitude. Within it, the wave amplitude grows exponentially as shown in the first ten units of time in figure 2(*a*) for $\beta = 1$. Immediately beyond it, the waves begin to steepen in front and develop a back shoulder, signifying a weakly nonlinear excitation of an overtone with wavelength $\frac{1}{2}\lambda_c$. The amplitude modulation due to the initial condition still persists, however, and the nonlinear convective effect begins to accelerate the larger waves. The relative speeds between the large waves are small. They collide and eventually overtake the smaller waves in front of them. However, its amplitude does not increase significantly as a result of these collisions. At the same time, smaller waves grow and interact with each other. The final result of the slow evolution is a train of soliton-like coherent structures with almost the same amplitude which interact indefinitely with each other like a soliton–soliton elastic collision. The coherent structure possesses a gently sloping back edge and a steep front edge preceded by some small 'bow waves' reminiscent of the solitary-wave coherent structures

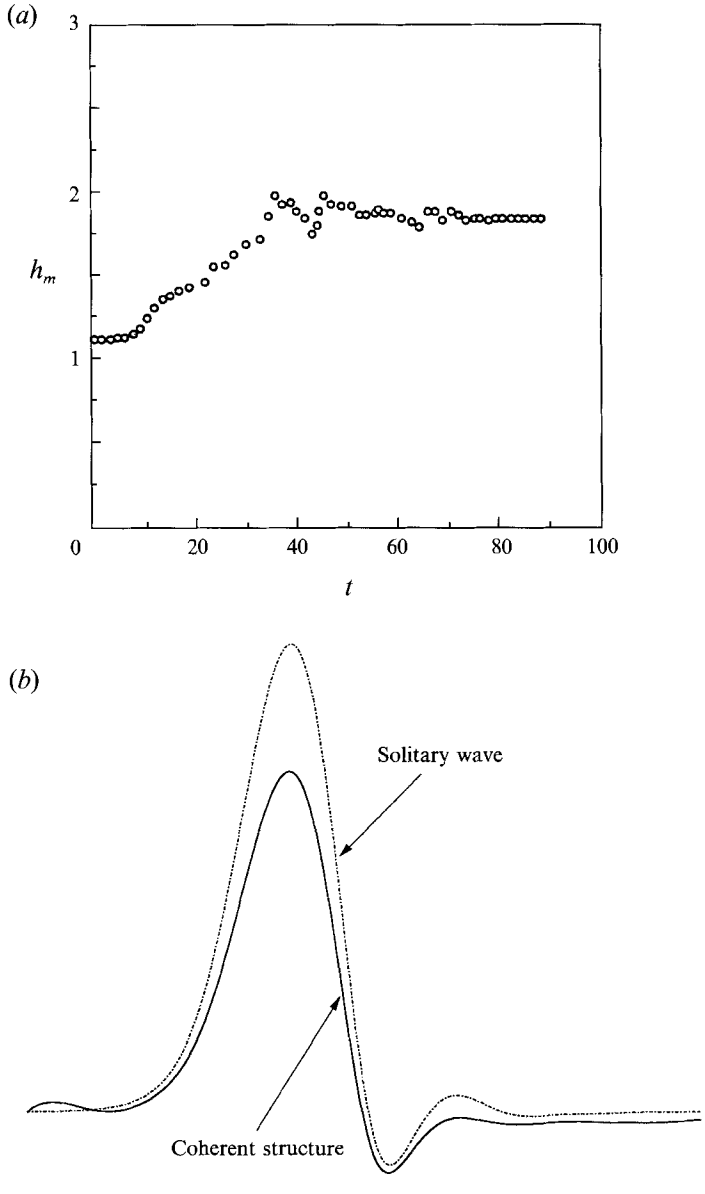

FIGURE 2. (*a*) The amplitude h_m evolution of one wave crest into a coherent structure of $\beta = 1 < \beta_c$ with a domain size of $L = 50$. The exponential growth in the linear inception region is followed by an algebraic growth period which includes coalescence with another wave crest and an asymptotic saturated interval where the slight fluctuations are due to decaying coherent structure interaction. (*b*) The final coherent structure compared to the numerically constructed solitary wave at $\beta = 1$.

observed in inertia-dominated falling films (Pumir *et al.* 1983; Chang 1986, 1989). However, unlike those coherent structures, the lateral dimension of the present structure scales as $\beta^{-\frac{1}{2}}$, that is the width remains of order R (or the Rayleigh wavelength λ_c) in the dimensional units. Since the height is scaled by the film thickness h_0 instead of R, the height of these coherent structures must be of the order $\epsilon^{-1} = \lambda_c/h_0$ before they escape the long-wave description. Consequently, even though the height of the coherent structure increases with β, they remain within the region of validity of (7). A

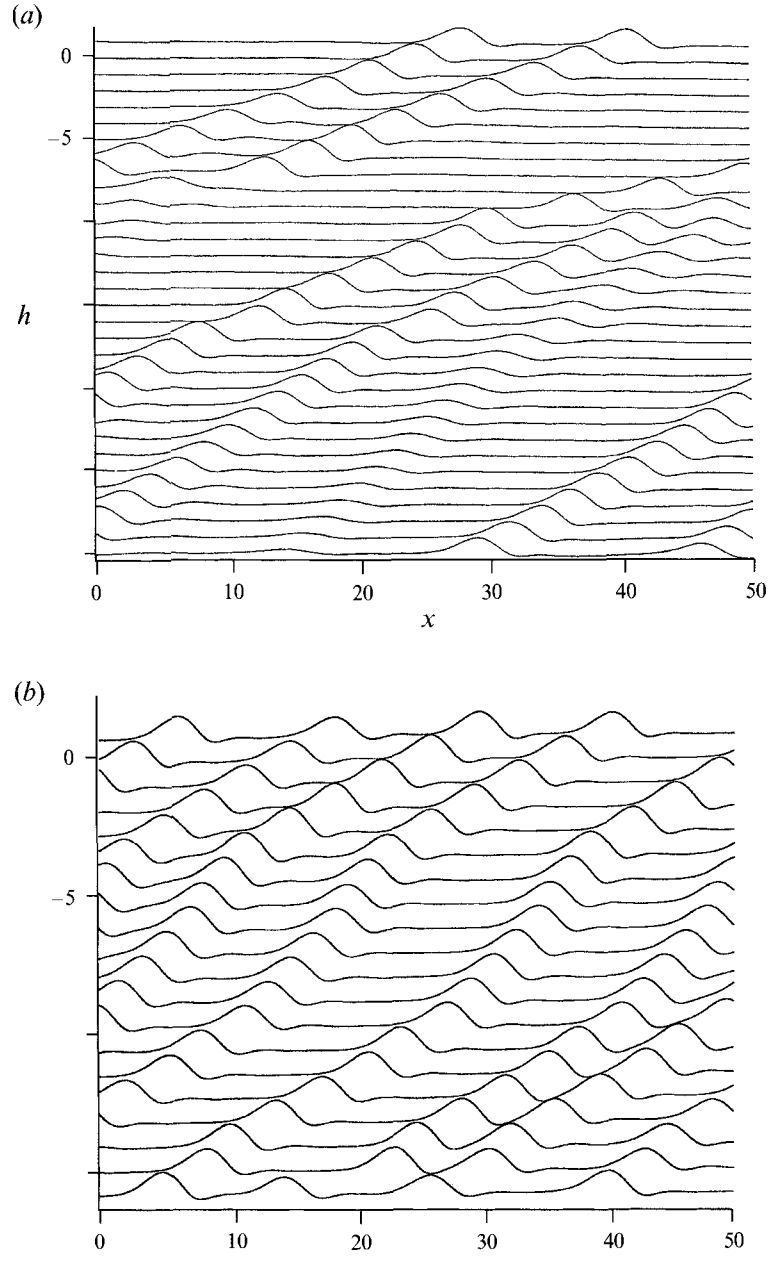

FIGURE 3. (*a*) The evolution towards two bounded coherent structures for a single-harmonic initial condition of $h(x,0) = 1-0.1\cos(2\pi x/L)$ with $L = 50$. The lines are separated by a time interval of $\Delta t = 0.70$ ranging from $t = 50.55$ to $t = 72.25$. (*b*) The asymptotic evolution towards a periodic train of coherent structures for an initial condition of $h(x,0) = 1-0.005\cos(2\pi x/L)$ with $L = 50$ for $t \in$ (71.5, 90.5) with $\Delta t = 1.0$.

typical large-time evolution ($t > 40$) of this coherent-structure dominated interface beyond the linear inception region is shown in figure 3(*a*) for $\beta = 1.0$. The snap shot of a fully developed coherent structure is shown in figure 2(*b*). In figure 3(*a*), the five wave crests ($L/\lambda_c \sim 5.6$) beyond the inception region have coalesced into two coherent structures which evolve into a closely bounded pair (a two-hump solitary wave) that

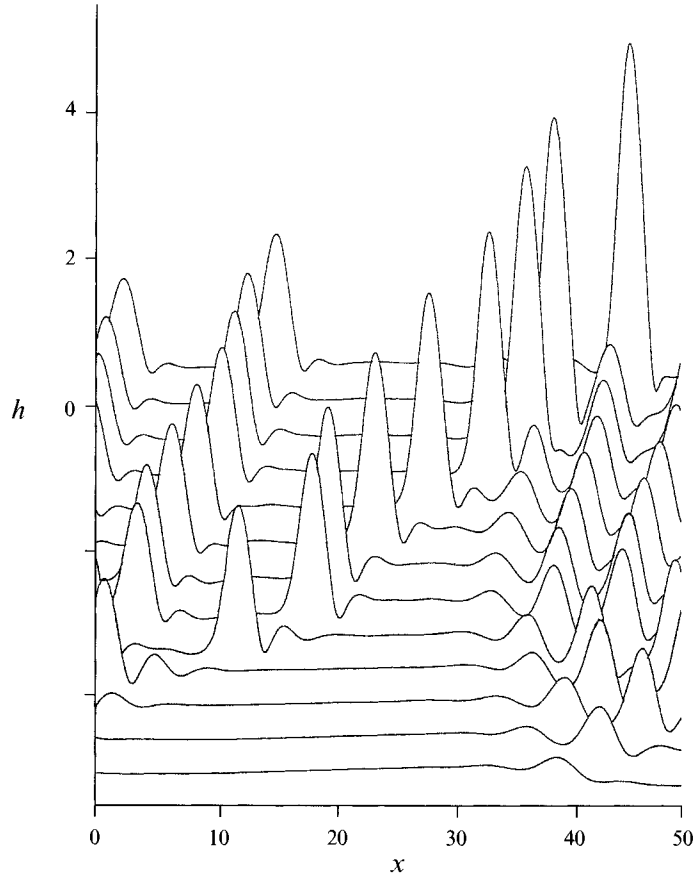

FIGURE 4. The local blow-up behaviour at $\beta = 1.6$ between the interval $t \in (7.0, 16.7)$ for $L = 50$.

propagates steadily without further evolution. The remaining domain away from the two localized structures is relatively flat with a slight modulation but linear inception of small waves does not occur over a timescale much larger than the inception time. The number of final coherent structures changes, however, with different initial condition. In figure 3(*b*), the final evolution for the same condition as figure 3(*a*) but with the initial condition $h(x, 0) = 1 - 0.005 \cos(2\pi x/L)$ yields four coherent structures which are spaced equally to form a periodic train. The interaction among the coherent structures is not necessarily stationary in a moving frame at large time. Dynamic interaction with continuously varying separation has been observed to persist indefinitely. However, once relaxed into the coherent structures, the structures do not coalesce and the interaction seems to be the type that neighbouring structures attract and repel alternately (Kawahara & Toh 1988). The unique feature of the dynamics for $\beta < 1.2$ is then the formation of such distinctive, indestructible coherent structures whose interaction dominates the final evolution. Since the amplitudes of these coherent structures are finite and unique for a given β value less than 1.2, this final evolution involves little vertical growth but consists entirely of lateral interaction. The nonlinear evolution beyond the linear inception region of the amplitude of a single crest towards the saturated amplitude of a coherent structure is shown in figure 2(*a*) and figure 5(*a*). A slow algebraic growth is evident and the decaying oscillations at large time are due to dynamic interaction among the coherent structures.

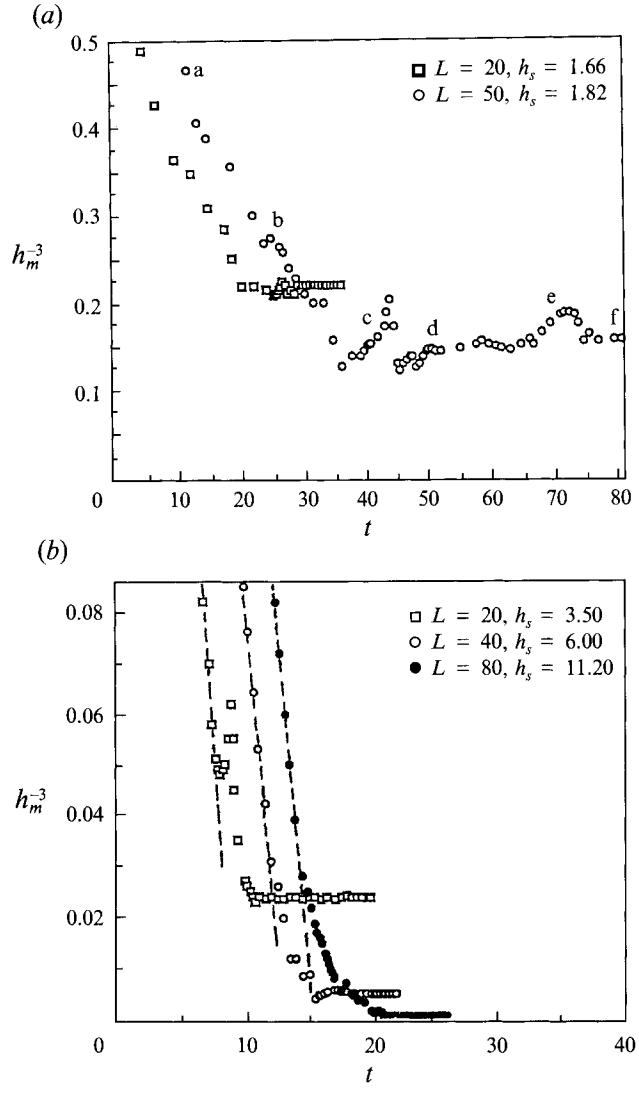

FIGURE 5. (*a*) Slow growth of the amplitude h_m of a typical wave crest at $\beta = 1.0$ without a self-similar region for the single-harmonic initial condition with an amplitude of 0.1. The eventual saturated amplitude h_s is a weak function of the domain size L. (*b*) Accelerated growth of the amplitude h_m of the dominant structure at $\beta = 1.8$ with a self-similar region for the same initial condition which converges to a local finite-time blow-up solution as L increases. The shift is due to the increasing inception interval with increasing wavelength of the single-harmonic initial condition. The saturated amplitude increases with L linearly.

The evolution is dramatically different when the same initial condition is used for β larger than approximately 1.6 as shown in figure 4. The dynamics of the linear inception region evolves as before. However, beyond the inception region, instead of coalescing with others to form saturated coherent structures, one of the wave crests of the periodic wave train begins to grow very rapidly. It dominates the other crests and, in fact, reduces the height of the other crests as fluid drains into this localized growing structure. The growth in amplitude h_m of this localized structure behaves as $h_m^{-3} \sim (t - t_0)$ as shown in figure 5(*b*) for $\beta = 1.8$ where the amplitude increased by a factor of 2 in a short time interval of about 2 units. In contrast, the crest height

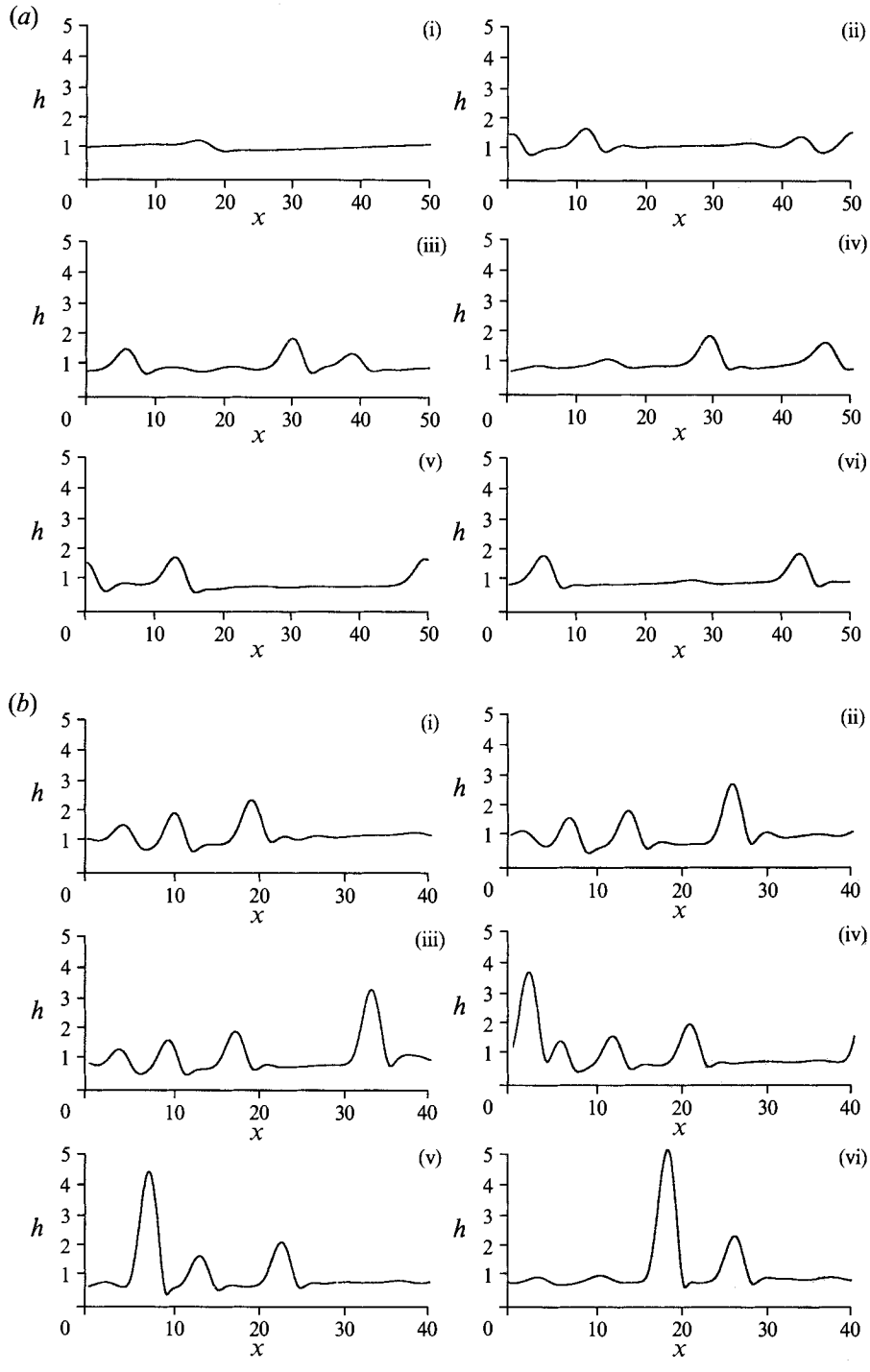

FIGURE 6. Snap shots of the interfacial shape at indicated points in figure 5. For $\beta = 1.0(a)$ the snap shots are at $t = 10.5$, 23.75, 40.25, 50.55, 71.05 and 80.175 and for $\beta = 1.8(b)$ at $t = 10.375$, 11.00, 12.0, 13.0, 13.5 and 14.5. The timescales are different by one order of magnitude.

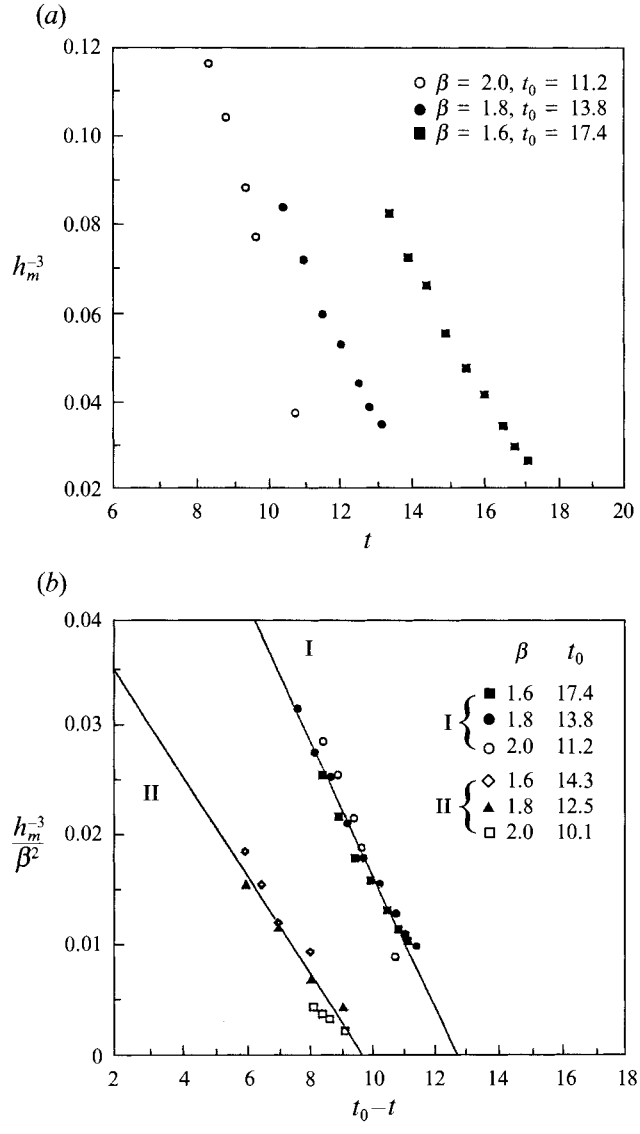

FIGURE 7. (*a*) The algebraic growth during the blow-up interval of the maximum amplitude towards blow-up at $t = t_0$ for the initial condition $h(x,0) = 1-0.1\cos(2\pi x/L)$ for three β values larger than β_c at $L = 50$. The estimate of t_0 from the plots are also shown. The eventual deviations from the blow-up behaviour are removed in this figure. (*b*) The normalized curves for various β values for two different initial conditions: I. $h(x,0) = 1-0.1\cos(2\pi x/L)$ and II. $h(x,0) = 1-0.2\cos(2\pi x/L)$. The slopes are $e = 6.0\times10^{-3}$ and 4.9×10^{-3}, respectively.

evolution for $\beta < 1.0$ shown in figure 5(*a*) does not demonstrate this self-similar growth and its fastest growth factor is only 1.3 over a much larger interval of 20 units! As a result, the growth of $\beta = 1.8$ is significantly faster by one order of magnitude as is evident from the timescales of figure 5. More detailed snapshots of both growth processes are shown in figure 6 where the self-similar growth of a dramatically large structure for $\beta = 1.8$ is contrasted to the small identical coherent structures of $\beta = 1.0$. Even at $\beta = 1.8$ with the largest domain size L, however, the self-similar intermediate asymptotic behaviour that leads to the large structure breaks down at large time as a

dimple develops in front of the structure and it becomes increasingly difficult to drain fluid through this small constriction. This dimple is already apparent in figure 6 and it deepens with further evolution. We believe the tail which departs from the self-similar growth in figure 5(*b*) is related to the lobe drainage mechanism through the dimple first studied by Hammond (1983). As L is increased, however, figure 5(*b*) suggests that the blow-up-like behaviour persists longer and the dimple does not develop as rapidly since there is more fluid available. The final saturated amplitude increases linearly with L, in contrast to the relative insensitivity of the final amplitude to L for $\beta = 1.0$ shown in figure 5(*a*). For $\beta = 1.8$, the saturated amplitudes are $h_s = 2.25$, 3.50, 6.0 and 11.2 for $L = 10$, 20, 40 and 80. This again suggests that a true blow up will occur in finite time if an infinite domain is used or if an artificial boundary condition that allows infinitely fast transfer of liquid into the domain is used. The tails that deviate from the blow-up behaviour exhibit kinks which correspond to coalescence of the large structure with smaller saturated ones. Such coalescence hence also plays a role in the final evolution of the drop in addition to the lobe drainage mechanism of Hammond. Since Hammond's lobes do not move owing to the absence of the mean flow term, coalescence is not observed in his analysis. Although the final coalescence and lobe drainage mechanisms contribute to the significant final increases in the crest height h_m of the growing structure as evident in figure 5(*b*), they must be preceded by the intermediate blow-up interval. Without the blow-up behaviour, as is the case for lower values of β, figure 5(*a*) indicates that the evolution is dominated by lateral interaction of the saturated coherent structures without amplitude growth. The intermediate blow-up interval is hence necessary for drop formation. This important interval possesses a self-similar property that allows the renormalization of all intermediate blow-up behaviour. Since t_0 obviously depends on the initial condition, we have chosen to renormalize various blow-up solutions by using t_0 as the origin of the time coordinate, that is using the timescale $t-t_0$, for any given run. The proper scaling of the blow-up interval is revealed by figure 7(*b*) when this shifted timescale is used on the raw data of figure 7(*a*). The amplitude blow up seems to be universal as t approaches t_0 with a scaling of β^{-2}

$$(h^{-3}/\beta^2) \sim e(t-t_0), \tag{22}$$

where $e = 6.0 \times 10^{-3}$ for the cosine initial condition with an amplitude of 0.1 from figure 7 but it varies with other initial conditions as shown in figure 7(*b*). In fact, even the profile of the blow-up structure away from the film approaches a constant shape if the $(t-t_0)^{-\frac{1}{3}}$ growth is normalized away and the residual translation of the structure during the blow-up process is frozen by matching the maxima at various time as in figure 8(*a*). The structure approaches the static solution (10) of the long-wave Laplace–Young equation. It seems to evolve through the family of the unduloid solution with algebraic growth.

We have also integrated (7) with numerous other initial conditions. In all cases, an approach towards a coherent-structure dominated interface occurs for $\beta \lesssim 1.2$ and blow-up-like growth occurs at a single crest for $\beta \gtrsim 1.6$. Between these two values, saturation at extremely large coherent structures occurs and it is difficult to discern whether a blow-up interval exists. Typical evolutions for $\beta = 0.8$ for a random initial condition whose local amplitude takes on a value between 0.85 and 1.15 are shown in figure 9(*a*). (The random initial condition is smoothed before numerical integration in time.) The accelerated growth at the larger value of $\beta = 1.8$ is again evident with final amplitudes in excess of 4, although two large structures are now apparent, suggesting that the existence and non-existence of the intermediate blow-up phenomenon are

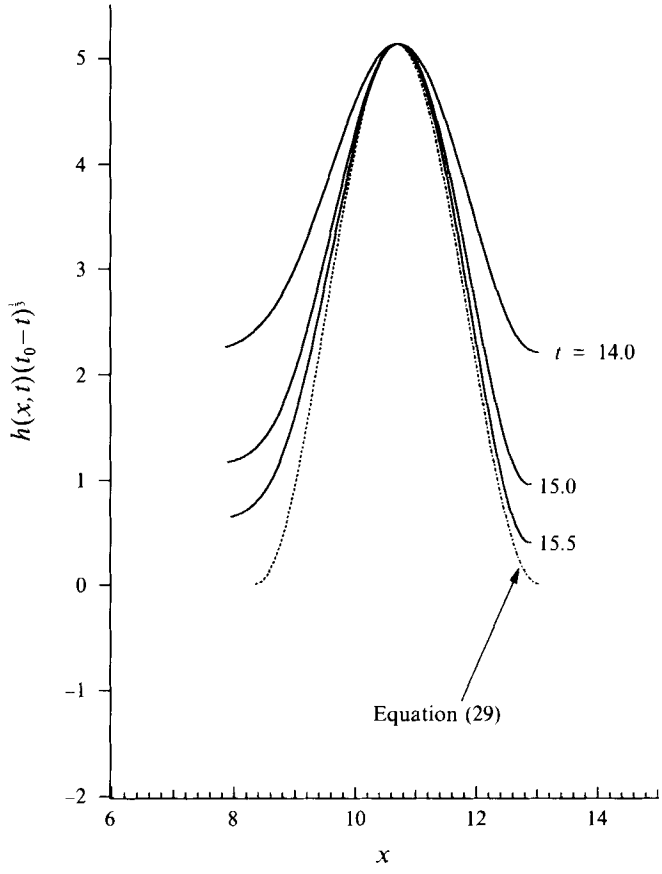

FIGURE 8. Approach of the transient blow-up solution for $\beta = 1.6 > \beta_c$ towards the static structure defined by equation (29). The asymptotic blow-up time is $t_0 = 17.4$.

independent of initial conditions. We have also used a family of solitary wave solutions to be constructed in a subsequent section as a family of initial condition for all β. As shown in figure 10, all numerical integrations for $\beta < 1.2$ yield saturated coherent structures while for $\beta > 1.6$, a significant blow-up interval is observed. During this blow-up process, the interface $h(x, t)$ does not vanish at any location. It is easy to show from (7), as Pumir *et al.* (1983) have shown for their equation, that a minimum of the interface can never touch the fibre unless h_{xx} or h_{xxxx} becomes singular such that the interface breaks into segments of piecewise continuous profiles. Singularity formation, corresponding perhaps to wave breaking, is also not observed. The combination of a large reservoir of fluid and a mean flow probably eliminate the possibility of dry patch formation. This is consistent with the experiment of Aul & Olbricht (1990) for an annular film within a capillary. With the introduction of a mean flow dry patches are not observed and instead, complete snap-off of the inner thread occurs as an occasional lobe sucks fluid from neighbouring lobes and blows up to form a fluid lens. This snap-off process is obviously related to the present drop formation process and one also expects a critical film thickness beyond which a lens can be formed. In fact, although the film is on the inside of a capillary instead of outside a fibre, this difference is negligible and we expect the evolution equation (7) and our prediction of the critical film thickness to be valid for the snap-off phenomenon.

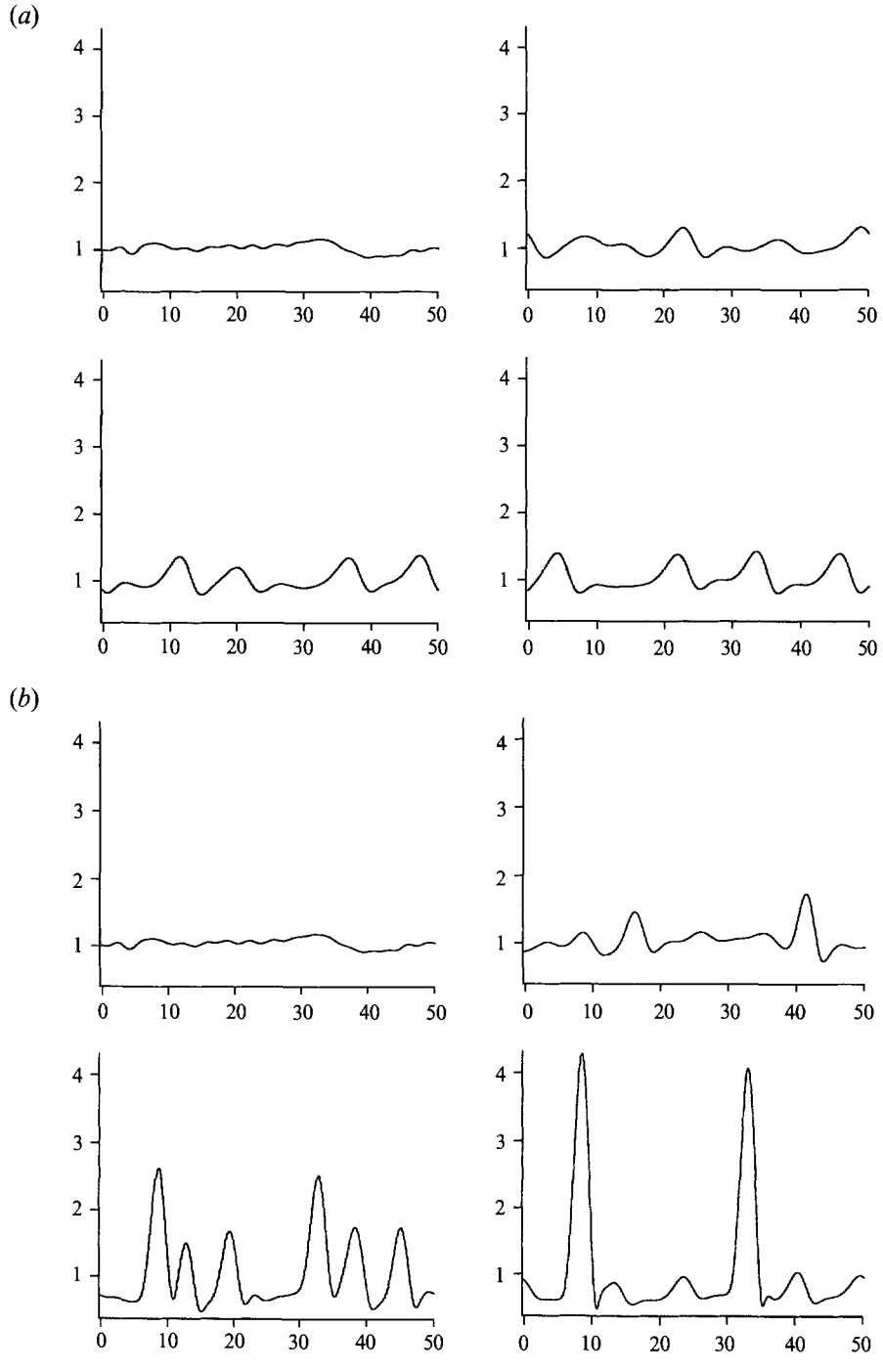

FIGURE 9. Evolution with random initial condition at $L = 50$ for (*a*) $\beta = 0.8$ at $t = 0$, 12.5, 26.6 and 134.6. (*b*) $\beta = 1.8$ at $t = 0$, 2.5, 6.3 and 9.4.

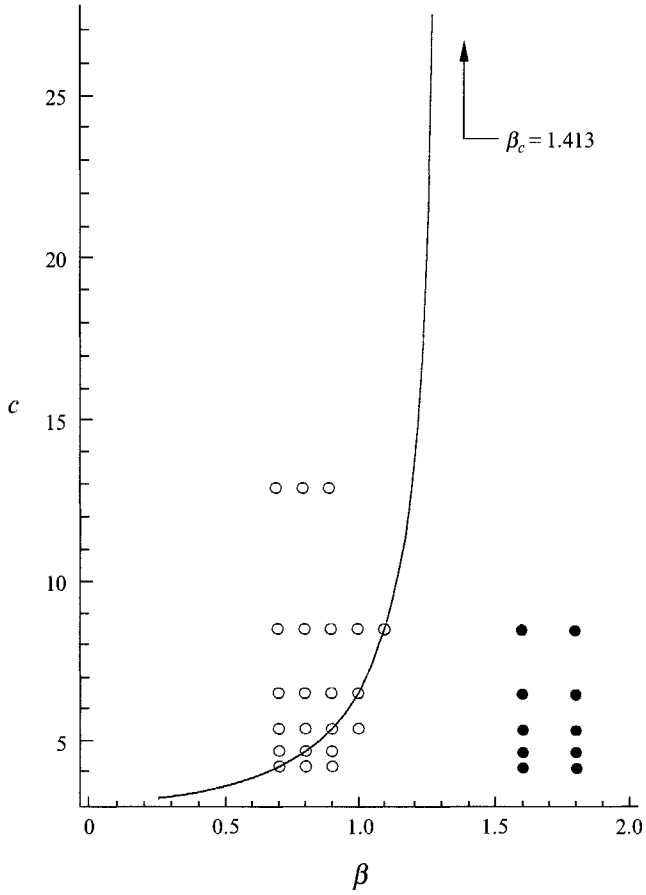

FIGURE 10. The computed solitary wave solution branch and the predicted singularity at $\beta_c = 1.413$. The open circles at (β, c) represent saturated long-term dynamics when the solitary wave solution with speed c is used as the initial condition at the given β while the closed circles represent observed self-similar intermediate asymptotic growth with the same initial conditions.

3. Finite-time blow up and solitary waves

The local and transient self-similar intermediate blow-up behaviour observed in our numerical study occurs as fluid drains preferentially into a single localized structure. The scaling properties of this phenomenon demonstrated in figures 7 and 8 suggest that this local blow-up behaviour can be described by an intermediate self-similar asymptotic solution to (7). We assume this finite-time blow up occurs at $t = 0$ at the location $x = 0$ and seek its shape and evolution behaviour. Defining a similarity independent variable $y = xt^{-b}$ and a transformation of dependent variable $h(x, t) = |t|^{-a}\eta\ (y)$, where a and b are positive, we shall find the appropriate similarity transform to reduce (7) to an ordinary differential equation for $\eta(y)$, as Pumir *et al.* (1983) have done for their equation. Direct substitution yields

$$-a\eta - by\eta_y + [|t|^{-2a-b+1}\eta^3 + \beta|t|^{-3a-2b+1}\eta^3\eta_y + |t|^{-3a-4b+1}\eta^3\eta_{yyy}]_y = 0.$$

Consequently, a self-similar solution exists near blow up ($t \to 0^-$) if $a = \frac{1}{3}$ and $b = 0$. The convective term $[|t|^{\frac{1}{3}}\eta^3(x)]_x$ vanishes as $t \to 0^-$ and the resulting equation for $\eta(x)$ is

$$-\tfrac{1}{3}\eta + \frac{\mathrm{d}}{\mathrm{d}x}[\beta\eta^3\eta_x + \eta^3\eta_{xxx}] = 0, \tag{23}$$

and the interface behaves as

$$h(x,t) \sim |t|^{-\frac{1}{3}}\eta(x). \tag{24}$$

This then confirms the $(t-t_0)^{-\frac{1}{3}}$ scaling for the blow-up process in figure 5(*a*). Even the universal scaling of figure 7(*b*) and (22) is now clear since the self-similar equation (23) is invariant to the transformation $\eta \to \beta^{-\frac{2}{3}}\eta$ and $x \to \beta^{-\frac{1}{3}}x$. Thus, $h_m = \eta_m t^{-\frac{1}{3}} \sim e^{-\frac{1}{3}}\beta^{-\frac{2}{3}}t^{-\frac{1}{3}}$ where the constant e is determined from figure 7(*a*) and (22) to be 6.0×10^{-3} for the cosine initial condition with 0.1 amplitude. Another value of e corresponding to a different initial amplitude is listed in figure 7(*b*). In general, the constant e must be determined from the transient version of (23). Its solution then requires matching with the initial condition. Hence, this constant is a function of the initial condition in general as demonstrated in figure 7(*b*).

While the determination of e requires information about the initial condition and hence a general analysis is not possible, the leading-order structure of the blow-up solution can still be deciphered. Mean flow effects have been eliminated from equation (23) and it represents a balance between the evolution term $-\frac{1}{3}\eta$ and static capillary forces. It essentially describes the algebraic evolution in time through the family of unduloidal static solutions of the Laplace–Young equation. In the original variables, the behaviour as $t \to 0$ of the blow-up process is then described by

$$\frac{\partial h}{\partial t} + [\beta h^3 h_x + h^3 h_{xxx}]_x = 0, \tag{25}$$

which is simply the equation studied by Hammond for the case without mean flow. Consequently, the blow-up solution is entirely driven by the static capillary forces which drain fluid from the surroundings to a single crest. Because the draining process is slow relative to the timescale for the linear Rayleigh instability used to scale time in (7), the growing crest evolves in a quasi-steady manner and takes on shapes described by (10) to leading order which approaches the fibre surface tangentially (see figures 4 and 8). This suggests that η is large in (23) and the boundary conditions to the leading-order outer solution (away from the quadratic tangent points) are

$$\eta^0(0) = 2D, \quad \eta^0_x(0) = \eta^0_{xxx}(0) = 0, \quad \eta^0(\pm\sigma) = \eta^0_x(\pm\sigma) = 0,$$

where $2D$ is the height of the blow-up solution at the maximum located at $x = 0$ and $\pm\sigma$ are the yet undetermined matching locations. (An analogous discussion on why these boundary conditions are appropriate for the leading-order equation can be found in §4 for the solitary waves.) It should be noted, however, that the boundary conditions in (26) correspond to the asymptotic behaviour of the 'outer' solution of the large structure $\eta(x)$ as it approaches the film. It cannot describe the small interfacial structures near the film nor does it take into account the boundary conditions of the domain. For example, the dimple that develops in figure 6, which eventually causes the deviation from the blow-up behaviour, obviously escapes the description of (26). Hence the constructed blow-up solution only pertains to a single wave crest and it is not a global blow-up solution in time for the original equation (7). In fact, as we have mentioned, (7) cannot exhibit blow up with periodic boundary conditions because of mass conservation. Consequently, one should look at the constructed solution as a necessary intermediate nonlinear growth mechanism for a local wave crest that follows the initial linear exponential growth and precedes the lobe drainage mechanism when the dimple is sufficiently deep to dominate the final evolution. Matching of the self-similar interval with these two regions would be a difficult task as we discuss below.

Since D is large, the leading-order outer solution can be easily shown to be

$$\frac{\mathrm{d}}{\mathrm{d}x}[(\eta^0)^3(\beta\eta^0_x+\eta^0_{xxx})]=0, \tag{27}$$

such that the evolution term $-\frac{1}{3}\eta$ is negligible. The solution to (27) which satisfies (26) is simply the long-wave Laplace–Young solution (10),

$$\eta^0(x)=D(1+\cos\beta^{\frac{1}{2}}x), \tag{28}$$

where the contact points are located at $x=\pm\sigma=\pm\pi/\beta^{\frac{1}{2}}$. The leading-order blow-up solution is then

$$h_b(x,t)=D(1+\cos\beta^{\frac{1}{2}}x)|t|^{-\frac{1}{3}}, \tag{29}$$

where D is obviously related to e in (22). We note that D is still unknown and it must be determined with higher-order matching which involves the evolution term $-\frac{1}{3}\eta$ and the transient convective term neglected in (23). This now requires information on the initial condition and is hence impossible to do in general. Nevertheless, the quasi-steady evolution through the unduloidal solutions of the Laplace–Young equation is evident from (29) and is confirmed by our numerical study in figure 8.

Whether the blow-up solution h_b can be approached locally by a particular wave crest, that is whether D can be determined after carrying out a proper matching with the initial conditions, is not guaranteed, however. In fact, we expect the nonlinear mean-flow effect contained in the asymmetric convective term to prevent an approach to the blow-up solution. In this connection, we consider yet another self-similar solution $H(z)$ to (7). This solution corresponds to a stationary solitary wave which propagates at speed c without changing its profile. This profile approaches the flat-film solution $H=1$ at both ends. It has a localized structure resembling the coherent structure in figure 2 with a capillary-force-dominated outer region and two matching regions with the flat film where both surface tension and viscous forces are expected to be dominant. It is described by the following equation in the moving coordinate with translation velocity c, $z=x-ct$,

$$H^3H_{zzz}+\beta H^3H_z=1-H^3+c(H-1), \tag{30a}$$

with boundary conditions

$$H(z\to\pm\infty)=1, \tag{30b}$$

where (7) has been integrated once in the moving frame and the integration constant is determined by the condition that $H=1$ must be a solution. The mean-flow convective term is now contained in $1-H^3$ while $c(H-1)$ corresponds to the viscous term owing to the propagation of the solitary wave. We are interested in large solitary waves which travel fast ($c\gg1$) and we shall carry out on expansion in $c^{-\frac{1}{3}}$ in the next section. We shall show that they correspond to the coherent structures in figures 2 and 3 and that it is possible to have extremely large solitary waves with dimensions of the fibre radius R at a limiting β value. They are possible owing to the mean-flow term. This will be shown to occur when $H\sim O(c^{\frac{2}{3}})$ and $z\sim O(1)$ such that the outer region of the solitary wave is again described by the long-wave Laplace–Young equation to the leading order,

$$\frac{\mathrm{d}}{\mathrm{d}z}[\beta H^3H_z+H^3H_{zzz}]=0. \tag{31}$$

The leading-order outer solution of the solitary wave solution (away from the thin film) is then

$$H=H_s[1+\cos\beta^{\frac{1}{2}}(x-ct)] \tag{32}$$

within the outer region confined by the two contact points $z_{\pm} = \pm\pi/\beta^{\frac{1}{3}}$ in the moving frame. Like D of the blow-up solution (29), H_s must be obtained from higher-order matching at the contact points. Unlike the blow-up solution, however, this steady matching is possible and will be carried out in the next section.

The resemblance of the two leading-order self-similar solutions in (29) and (32) is important. Both are possible attractive intermediate asymptotic solutions to a particular wave crest with their own domains of attraction but with very different behaviour – one blows up in finite time to leading order until higher-order terms due to film thinning become important and one translated without growth. Actually, a true solitary wave in an infinite domain is unstable and hence has no domain of attraction because of the extended flat film region. We are actually referring to attractors (see figure 3) which are dominated by solitary-wave-like coherent structures. We shall show subsequently that the unstable solitary wave can generate a countable infinite family of coherent-structure-dominated asymptotic solutions, a subset of which do have finite domains of attraction and hence compete locally at a particular wave crest with the blow-up solution. For now, however, we shall consider the solitary wave as an attracting asymptotic solution for simplicity. Its resemblance to the blow-up solution suggests that they compete directly at a specific wave crest and that both cannot be attracting. Consider the blow-up solution at a particular instant in time t before blow up such that $D\,|t|^{-\frac{1}{3}}$ is identical to H_s of (32) which is always possible for a sufficiently large H_s. The profile at that instant can then continue to evolve upwards in the blow-up process. Alternatively, since it also satisfies (32) with $t = 0$, it can also translate as a solitary wave. This is obviously impossible and the blow-up solution and a solitary wave solution cannot both be attracting for a given β. In all our numerical studies, we find that the solitary wave is always the chosen one and the blow-up solution is never reached. Figure 5(*a*) for $\beta = 1.0$ clearly shows the dominance of the solitary-wave solution over the blow-up solution which is evident in figure 5(*b*). This then implies that if the solitary wave solution exists, it will always rapidly dominate and eliminate the blow-up behaviour. We then seek to determine the critical β_c beyond which solitary waves do not exist as a condition for prolonged blow up into drops. As we shall demonstrate, solitary waves exist as a bounded, steady solution because the mean flow balances the capillary growth in the moving coordinate. This saturation is only possible if the solitary wave translates at a specific velocity. It is hence the same physical mechanism that prevents blow up. We have, however, replaced the difficult task of determining D in (29) through matching with the initial condition with the task of estimating H_s and c in (32) by matching with the two steady viscous films on both sides of the solitary wave. We expect the solitary wave amplitude $H_s(\beta)$ and speed $c(\beta)$ to increase as β increases. At a critical β_c, the capillary force is too strong to be arrested by the mean-flow effects and we expect both H_s and c to approach infinity (see figure 10).

Although the solitary-wave solution is strictly unstable, other self-similar solutions that are attractive can be generated from the solitary-wave solution. Some of these solutions correspond to stationary solutions in a moving frame which satisfy (30*a*) but not necessarily (30*b*). The existence of these subsidiary stationary solutions with structures resembling the true solitary wave can be shown by use of the Sil'nikov theorem from dynamical systems theory (Chang *et al.* 1993*a*). Equation (30*a*) for stationary waves can be converted into a three-dimensional dynamical system (Ratulowski & Chang 1989),

$$\boldsymbol{u}_x = \boldsymbol{f}(\boldsymbol{u}; c, \beta), \tag{33}$$

by the transformation $(u_1, u_2, u_3) = (H-1, H_z, H_{zz})$. We note that the flat-film solution

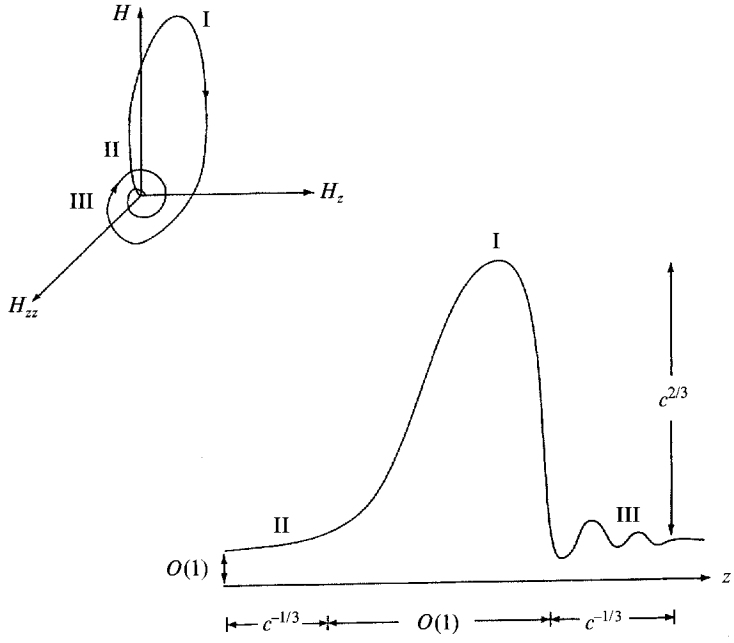

FIGURE 11. The scalings of the solitary wave with respect to the wave velocity c and the analogue homoclinic orbit in the phase space.

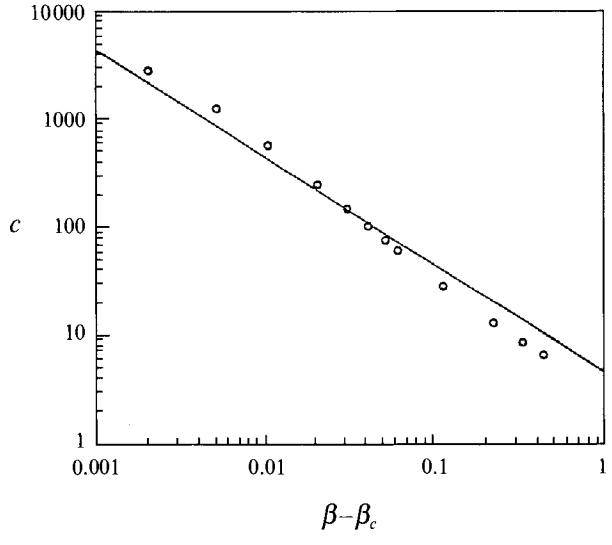

FIGURE 12. The computed solitary wave speeds in figure 7 near $\beta = \beta_c$ compared to the derived asymptotic behaviour shown as a straight line.

$(H-1, H_z, H_{zz}) = (0,0,0)$ becomes now a fixed point of this dynamical system and the solitary-wave solution a homoclinic orbit that connects to this fixed point (see figure 11 for a schematic and figure 13 for some of our constructed homoclinic orbits/solitary waves). Linearization of the dynamical system about the fixed point yields a Jacobian whose spectrum is described by the characteristic equation

$$\lambda^3+\beta\lambda-(c-3)=0. \tag{34}$$

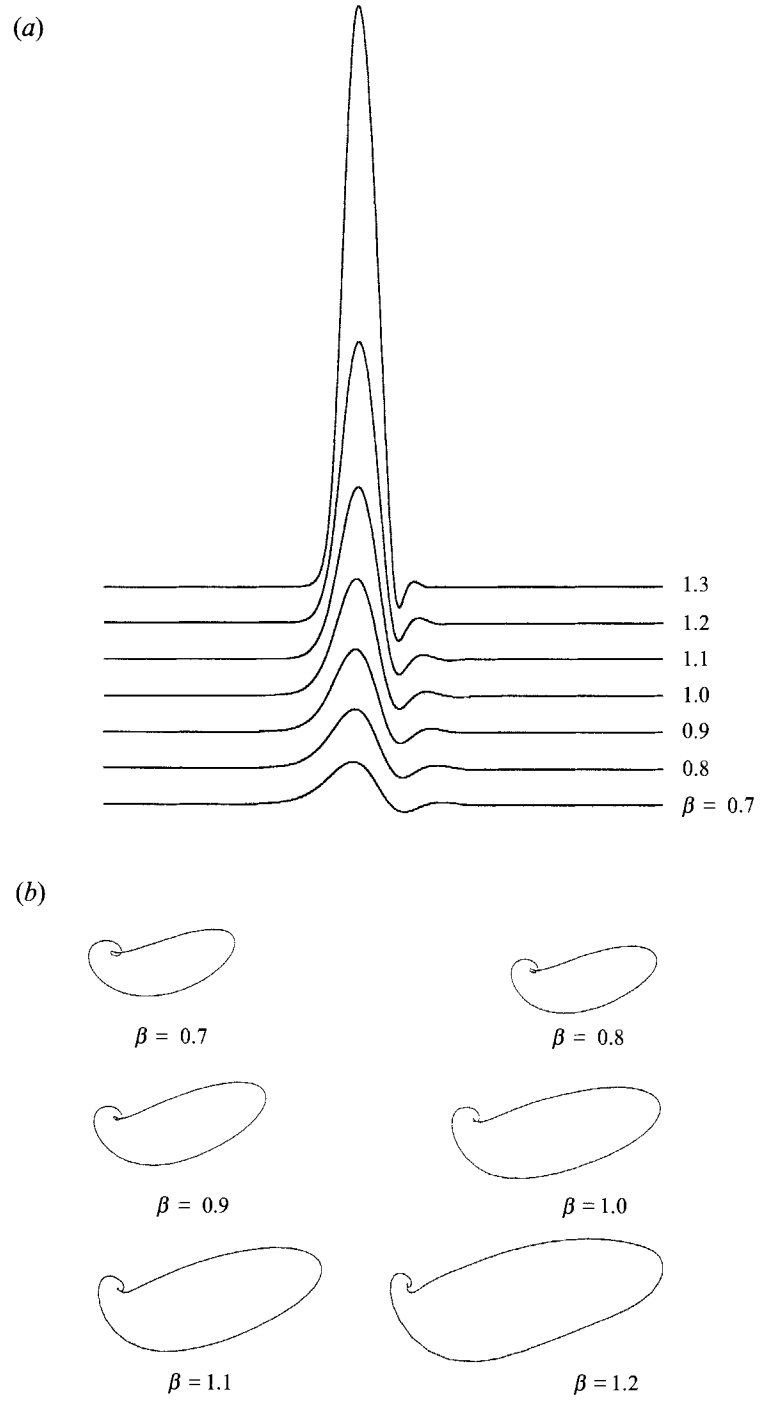

FIGURE 13. The numerically constructed family of solitary waves (*a*) and homoclinic orbits (*b*).

For $c-3>0$, which is always true since the solitary waves travel faster than the linear phase speed 3 (see Chang 1989), it is easy to show that one root of (34) is always real and positive and the other two roots are complex conjugates with negative real parts. Hence the homoclinic orbit leaves the fixed point monotonically along a one-dimensional unstable manifold but returns to it in an oscillatory fashion on a two-

dimensional stable manifold. Associating the flow in the phase space with the evolution of the solitary wave shape in z in the moving frame, one sees in figure 11 that the spectrum reflects the unique shape of the coherent structure observed on falling films, even in the inertia dominated case studied by Pumir *et al.* (1983) and Chang (1989). It has a gentle, monotonically increasing back edge preceded by a steeper front edge which is relaxed by a series of small, decaying bow waves which correspond to the complex eigenvalues. The asymmetric shape is a nonlinear effect away from the fixed point and is hence not related to the spectrum. It is in fact caused by the asymmetric convective term $(h^3)_x$ due to mean flow as we shall show in our nonlinear analysis in the next section. For small-amplitude solitary waves with $c-3$ small (we shall show that the speed of the solitary wave increases with amplitude), the complex pair is almost purely imaginary with frequency $\beta^{\frac{1}{2}}$. Hence, for small solitary waves, the bow waves decay slower and have longer wavelengths. In fact, as $c-3$ approaches zero, they correspond to the linear Rayleigh waves with wavelength λ_c of (1). These observations are consistent with our computed solitary waves in Figures 12 and 13. According to the Sil'nikov theorem (Glendinning & Sparrow 1984), if a homoclinic orbit exists at $(\beta, c) = (\beta^*, c^*)$, then a countable infinite number of limit cycles and subsidiary homoclinic orbits, like multi-hump solitary waves, also exist in a local neighbourhood of (β^*, c^*) in the parameter space provided if the real eigenvalue of (34) is larger in magnitude than the real part of the complex pair. Since the quadratic term in the characteristic polynomial is zero, the trace of the Jacobian vanishes and the above ratio is exactly 2 for any (β^*, c^*). Consequently, the Sil'nikov condition is satisfied and at a given β, we expect an entire family of stationary solutions, some periodic in z and some are multi-hump solitary waves, with speeds c close to the solitary wave speed. These solutions resemble the solidary waves – a periodic wave generated by this wave resembles a solitary wavetrain and a multi-hump solitary wave resembles two bounded solitary waves. All the subsidiary solitary waves are unstable but the periodic stationary waves can be stable. The subsidiary solitary waves can also give rise to periodic waves of their own. These stable stationary asymptotic states are evident in figure 3. Non-stationary attractors are also expected if the primary solitary wave exists. However, a general condition for their existence like the Sil'nikov theory is currently unavailable (see, however, the approaches of Kawahara & Toh, 1988 and Elphick, Meron & Spiegel 1988). It is then clear that, although the primary solitary wave itself is strictly unstable, it generates an infinite number of stable stationary and non-stationary attractors that compete with the blow-up solution. Since these subsidiary attractors have coherent structures resembling the solitary wave, their leading-order outer solutions are also described by (32) and they hence prevent the approach towards the blow-up solution by the same argument.

4. Construction of solitary waves

We seek an analytical solution of the nonlinear eigenvalue problem defined by the solitary wave equation (30). For a given β (or c), there is a unique c (or β) such that the boundary conditions (30*b*) are satisfied and a solitary wave (homoclinic orbit) exists. That only one parameter needs to be varied (a codimension one phenomenon) is due to the fact that the homoclinic orbit corresponds to the intersection of a two-dimensional stable manifold with a one-dimensional unstable manifold in a three-dimensional phase space. The solitary-wave solution branch is hence a one-parameter family and one can represent it by $c(\beta)$. The wave speed c is expected to approach infinity at a critical β_c beyond which the solitary-wave branch ceases to exist (figure 10).

We note that this approach to infinity of c at a finite β is different from the inertia-dominated solitary waves studied by Pumir *et al.* (1983). In the latter case, the solitary wave branch also ceases to exist beyond a critical parameter value but the singularity there is a limit point variety. We shall exploit the particular singularity here to carry out an analytical estimate of β_c and, in fact, to prove the existence of the singularity. Since both c and the wave amplitude approach infinity from below at β_c, we expand β as

$$\beta \sim \beta_c + \beta_1 c^{-\gamma} + \beta_2 c^{-2\gamma} + \beta_3 c^{-3\gamma} + \ldots, \tag{35}$$

and use some power of $1/c$ as the expansion parameter. The power γ will be determined from the scaling arguments. Even though the wave amplitudes are large near β_c, conditions (30*b*) still stipulate that two thin-film regions exist in the front and back of the peak. There are hence three regions of interest near βc, the outer region I, near the wave peak and the two inner film regions II and III in figure 11, whose solutions must be matched in a matched asymptotic analysis at the overlap region. In the inner regions, H is of order unity and we expect axial curvature and viscous terms to balance in (30). (The mean flow term $(1-H^3)$ is much smaller than the viscous term $c(H-1)$ since c is large). This dominant balance stipulates that the axial lengthscale must be of the order $c^{-\frac{1}{3}}$ and we define the inner coordinates

$$y = zc^{\frac{1}{3}}, \tag{36}$$

and write (30) as

$$H^3 H_{yyy} + \beta\delta^2 H^3 H_y = \delta^3(1-H^3) + (H-1), \tag{37}$$

where

$$\delta = c^{-\frac{1}{3}} \ll 1$$

will be the expansion parameter. Expanding H in powers of δ,

$$H = \sum_{i=0}^{\infty} \delta^i H_i,$$

we find that the leading-order equation is the Bretherton equation (Bretherton 1961) owing to the dominant balance of viscous and axial capillary terms,

$$\dddot{H}_0 = (H_0 - 1)/H_0^3, \tag{38}$$

where the dot denotes the derivative with respect to y.

This equation applies both at the back film II and front film III (see also the phase space locations in figure 11). In the back, one integrates (38) away from the flat-film solution $H_0 = 1$ in the positive y-direction whereas integration in the negative y-direction is required for the front. Equation (38) has been analysed using the Dynamical Systems language by Ratulowski & Chang (1989). The forward integration ($y \to +\infty$) quickly approaches the one-dimensional unstable eigen vector provided the initial condition is sufficiently close to the fixed point corresponding to $H_0 = 1$. It then follows the unstable eigen vector into the one-dimensional unstable manifold of (38) as nonlinear effects become important. Close to β_c, the eigen vector and unstable manifold of (38) are good approximations of those for (37) shown in figures 11 and 12(*b*). To eliminate the initial transient due to contributions from the stable complex modes, one can initiate the forward integration exactly on the unstable eigen vector or, equivalently,

$$H_0 \sim 1 + \epsilon_0^+ \exp(Y), \tag{39}$$

where Y and y is related by an arbitrary shift of origin

$$Y = y + r^+. \tag{40}$$

Using different initial amplitude ϵ_0^+, one obtains different asymptotic behaviour from (38) as $Y \to +\infty$. However, since the asymptotic trajectory in the phase space is invariant to shifts in y, these different trajectories collapse into one after shifting Y by a different interval r^+ according to ϵ_0^+ such that the origin of the new coordinate y lies at a particular point in the phase space which will be shown by matching to be located at the intersection of the asymptotic trajectory with the plane $H_y = 0$. We hence choose an arbitrarily small ϵ_0^+ (10^{-4} to be specific) and allow the matching to specify r^+ and the origin. Other choices of ϵ_0^+ lead to other r^+ but since the matching occurs at a specific location in the phase space and not in Y, the final results are invariant to the choice of ϵ_0^+. This procedure for the forward ($y \to +\infty$) matched asymptotic analysis of the Bretherton equation was first formalized by Park & Homsy (1984). The asymptotic behaviour in the backward direction ($y \to -\infty$) must be obtained with more care. Since the stable eigen space corresponding to (38) is two-dimensional, there are two eigenvectors with two independent amplitudes for initiating the integration in the negative y-direction. However, since the eigen values are complex conjugates, one of the amplitudes can be absorbed into a phase variable θ_0,

$$H_0 \sim 1 + \epsilon_0^- \exp(-\tfrac{1}{2}Y)\cos\left(\frac{\sqrt{3}Y}{2} + \theta_0\right), \tag{41}$$

where Y is again related to the properly reduced coordinate y by

$$Y = y + r^-. \tag{42}$$

The asymptotic behaviour at ($y \to -\infty$) is now determined by ϵ_0^- and θ_0. However, the final result is again invariant to ϵ_0^- provided the coordinate shift (42) is properly carried out and we choose ϵ_0^- to be 10^{-4}.

Higher-order inner equations can be derived from (37),

$$\dddot{H}_1 = (3 - 2H_0)\, H_1 / H_0^4, \tag{43}$$

$$\dddot{H}_2 = -\beta_c \dot{H}_0 + (3 - 2H_0)\, H_2 / H_0^4 - 3(2 - H_0)\, H_1^2 / H_0^5. \tag{44}$$

The solution to the linear equation (43) which satisfies the boundary condition $H_1(y \to \pm\infty)$ from (30*b*) is simply

$$H_1 = 0. \tag{45}$$

This can also be confirmed more rigorously from the matching. The next non-trivial inner solution is then H_2 and its integration in the forward direction should be initialized with

$$H_2 \sim (\epsilon_2^+ + \beta_c \epsilon_0^+ / 3)\exp(Y) - \tfrac{1}{3}\beta_c \epsilon_0^+ Y \exp(Y), \tag{46}$$

corresponding to a generalized stable eigenvector for the linearized version of the coupled system (38) and (44). One expects the leading-order asymptotic trajectory of the forced (non-autonomous) system (44) will also be invariant to a coordinate shift provided the coordinate Y in (46) is the same as that used in the leading-order analysis of (39). Similarly, integration in the backward direction should be initialized by

$$\begin{aligned} H_2 \sim\ & \exp(-Y/2)\cos(\sqrt{3}\,Y/2)\left[-\tfrac{1}{6}\beta_c \epsilon_0^- \cos\theta_0 - \tfrac{5}{18}\sqrt{3}\,\beta_c \epsilon_0^- \sin\theta_0 + \epsilon_2^- \cos\theta_2\right] \\ & + \exp(-Y/2)\sin(\sqrt{3}\,Y/2)\left[-\tfrac{\sqrt{3}}{18}\beta_c \epsilon_0^- \cos\theta_0 + \tfrac{1}{6}\beta_c \epsilon_0^- \sin\theta_0 - \epsilon_2^- \sin\theta_2\right] \\ & + Y\exp(-Y/2)\cos(\sqrt{3}\,Y/2)\left[\tfrac{1}{6}\beta_c \epsilon_0^- \cos\theta_0 - \tfrac{1}{6}\sqrt{3}\beta_c \epsilon_0^- \sin\theta_0\right] \\ & + Y\exp(-Y/2)\sin(\sqrt{3}\,Y/2)\left[-\tfrac{1}{6}\beta_c \epsilon_0^- \sin\theta_0 - \tfrac{1}{6}\sqrt{3}\beta_c \epsilon_0^- \cos\theta_0\right], \end{aligned} \tag{47}$$

corresponding to the generalized stable eigenvectors of the linearized version of (38) and (44). In principle, there are two independent generalized eigenvectors represented

by two independent parameters ϵ_2^- and θ_2, corresponding to the generalized versions of the two eigenvectors in (41) which are represented by ϵ_0^- and θ_0. However, θ_0 will be shown to be specified by matching and the generalized eigenvector of (46) must then correspond to the specific eigenvector in (41). In the polar coordinates used, this can be accomplished by simply requiring

$$\theta_2 = \theta_0. \tag{48}$$

By integrating (38) and (44) in both the forward and backward directions with initial conditions (39), (41), (46), (47) and for a given set of ϵ_0^+, ϵ_0^-, θ_0, ϵ_2^+ and ϵ_2^-, one obtains

$$H_0(Y \to \pm\infty) \sim a_0^\pm + b_0^\pm\, Y + d_0^\pm\, Y^2, \tag{49a}$$

$$H_2(Y \to \pm\infty) \sim a_2^\pm + b_2^\pm\, Y + (d_2^\pm - \tfrac{1}{2}\beta_c a_0^\pm)\, Y^2 - \tfrac{1}{6}\beta_c b_0^\pm\, Y^3 - \tfrac{1}{12} d_0^\pm\, \beta_c\, Y^4. \tag{49b}$$

For the asymptotic behaviours of H_0, d_0^+ is independent of the above five parameters (our integration yields $d^+ = 0.32152$ which is more accurate than Bretherton's and Ratulowski & Chang's values), a_0^+ and b_0^+ are functions of ϵ_0^+ only and a_0^-, b_0^- and d_0^- are all functions of ϵ_0^- and θ_0. For H_2, all the coefficients in the $+y$-direction (with $+$superscripts) are functions of ϵ_0^+ and ϵ_2^+ while all coefficients in the $-y$-direction are functions of ϵ_0^-, θ_0 and ϵ_2^-. One can replace ϵ_0^+ by r^+ and ϵ_0^- by r^- by using the coordinate shifts (40) and (42) to yield

$$H_0 \sim \hat{a}_0^\pm + \hat{b}_0^\pm\, y + d_0^\pm\, y^2, \tag{50a}$$

$$H_2 \sim \hat{a}_2^\pm + \hat{b}_2^\pm\, y + \hat{d}_2^\pm\, y^2 + \hat{e}_2^\pm\, y^3 + \hat{f}_2^\pm\, y^4, \tag{50b}$$

where

$$\begin{aligned}
\hat{a}_0^\pm &= a_0^\pm + b_0^\pm\, r^\pm + d_0^\pm (r^\pm)^2,\\
\hat{b}_0^\pm &= b_0^\pm + 2 d_0^\pm\, r^\pm,\\
\hat{a}_2^\pm &= a_2^\pm + b_2^\pm\, r^\pm - \tfrac{1}{6}\beta_c b_0^\pm (r^\pm)^3 + (d_2^\pm - \tfrac{1}{2}\beta_c a_0^\pm)(r^\pm)^2 - \tfrac{1}{12} d_0^\pm\, \beta_c (r^\pm)^4,\\
\hat{b}_2^\pm &= 2(d_2^\pm - \tfrac{1}{2}\beta_c a_0^\pm)\, r^\pm - \tfrac{1}{2}\beta_c b_0^\pm\, (r^\pm)^2 + b_2^\pm - \tfrac{1}{3}\beta_c d_0^\pm\, (r^\pm)^3,\\
\hat{d}_2^\pm &= d_2^\pm - \tfrac{1}{2}\beta_c a_0^\pm - \tfrac{1}{2}\beta_c b_0^\pm\, r^\pm - \tfrac{1}{2} d_0^\pm\, \beta_c (r^\pm)^2,\\
\hat{e}_2^\pm &= -\tfrac{1}{6}\beta_c b_0^\pm - \tfrac{1}{3}\beta_c d_0^\pm\, r^\pm = -\tfrac{1}{6}\beta_c \hat{b}_0^\pm,\\
\hat{f}_2^\pm &= -\tfrac{1}{12} d_0^\pm\, \beta_c.
\end{aligned}$$

In transforming to (50), we need to fix ϵ_0^+ and ϵ_0^- at the specific small values of 1.0×10^{-4}. The coefficients in (50) are then functions of $r^\pm$, θ_0 and $\epsilon_2^\pm$. These 5 quantities along with β_c, β_1, β_2 and β_3 from (35) will be determined by the matching conditions. Higher-order inner equations are not required.

The appropriate scaling for the outer region can be derived by scaling requirements necessary to match the asymptotic behaviour of the inner region. We first focus on the back matching with region II. The inner region behaves quadratically, $H_0 \sim y^2$, as $y \to \infty$ here and this then requires the outer solution Φ_0 to also behave quadratically with respect to the outer coordinate Z, $\Phi_0 \sim Z^2$. This simply states that the leading-order outer solution touches the fibre wall tangentially in the overlap region where it matches the asymptotes of the inner solution. Assuming the scaling $\Phi = Hc^a$ and $Z = zc^b$ in (30) where a and b are both non-positive since the length scales in the outer region are larger, one obtains from (30)

$$c^{-4a+3b}\Phi^3\Phi_{zzz} + \beta c^{-4a+b}\Phi^3\Phi_z = 1 - c^{-3a}\Phi^3 + c(c^{-a}\Phi - 1). \tag{51}$$

The requisite quadratic tangency of Φ_0 as it approaches zero to match the inner asymptotes in region II then stipulates that $a = 2b - \frac{2}{3}$ if one substitutes the inner scale (36) into the asymptotic form $\Phi \sim Z^2$. The two dominant capillary terms on the left-

hand side of (51) yield nonsensical solutions that cannot match both inner solutions if one dominates over the other. This then suggests a dominant balance of the axial and azimuthal curvature terms in the outer region which stipulates that b vanishes exactly and $a = -\frac{2}{3}$. The lateral lengthscale is then $O(1)$ in the outer region and the vertical one is $O(c^{+\frac{2}{3}})$ as shown in figure 11. Note that this apparently large aspect ratio does not violate the lubrication approximation because (30) has been rescaled. The appropriate equation for the outer region is then

$$\Phi^3\Phi_{zzz} + \beta\Phi^3\Phi_z = \delta^8 - \delta^2\Phi^3 + \delta^3\Phi - \delta^5, \tag{52}$$

where it is now clear from the outer equation (52) and the inner equation (37) that the expansion of β in (35) should be in powers of $\delta = c^{-\frac{1}{3}}$, that is $\gamma = \frac{1}{3}$. The leading-order outer equations are then, after expanding $\Phi \sim \Phi_0 + \delta\Phi_1 + \delta^2\Phi_2 + \delta^3\Phi_3$,

$$\Phi_0^3(\Phi_0''' + \beta_c\Phi_0') = 0, \tag{53a}$$

$$\Phi_0^3(\Phi_1''' + \beta_c\Phi_1' + \beta_1\Phi_0') = 0, \tag{53b}$$

$$\Phi_0^3(\Phi_2''' + \beta_c\Phi_2' + 1 + \beta_1\Phi_1' + \beta_2\Phi_0') = 0, \tag{53c}$$

$$\Phi_0^3(\Phi_3''' + \beta_c\Phi_3' + \beta_1\Phi_2' + \beta_2\Phi_1' + \beta_3\Phi_0') = \Phi_0, \tag{53d}$$

where the primes here denote derivatives with respect to z. We note that the $+1$ term in (53c) arises from the mean-flow term $\delta^2\Phi^3$ in (52). Since it is the mean flow effect that yields finite-amplitude solitary waves, we expect the analysis to at least extend to Φ_2 in region I. We shall require the solutions to (53) in this region to match asymptotically with the solutions (50) in regions II and III,

$$\delta^2 H(y \to \pm\infty) \sim \Phi(z = \delta y). \tag{54}$$

The solution of the leading order outer equation (53a) is simply

$$\Phi_0 = A_0\cos((\beta_c)^{\frac{1}{2}}z) + B_0\sin((\beta_c)^{\frac{1}{2}}z) + D_0, \tag{55}$$

and it defines the contact points

$$z_\pm = \pm\pi(\beta_c)^{\frac{1}{2}}, \tag{56}$$

which are the only locations where the requisite quadratic tangency can occur. They are essentially $\pm\sigma$ and $z_\pm$ is (26) and (32), respectively, near the critical point β_c. Expanding Φ_0 about these contact points and matching to H, one obtains

$$\Phi_0(z^\pm) = -A_0 + D_0 = 0, \quad \Phi_0'(z^\pm) = -(\beta_c)^{\frac{1}{2}}B_0 = 0, \tag{57a,b}$$

$$\frac{1}{2!}\Phi_0''(z^\pm) = \tfrac{1}{2}A_0\beta_c = d_0^\mp, \quad \frac{1}{3!}\Phi_0'''(z^\pm) = \frac{1}{3!}B_0\beta_c^{\frac{3}{2}} = 0, \tag{57d,e}$$

$$\frac{1}{4!}\Phi_0^{\mathrm{IV}}(z^\pm) = -\frac{1}{4!}A_0\beta_c^2 = -\tfrac{1}{12}\beta_c d_0^\mp, \quad \frac{1}{5!}\Phi_0^{\mathrm{V}}(z^\pm) = -\frac{1}{5!}B_0\beta_c^{\frac{5}{2}} = 0. \tag{57e,f}$$

Consequently,

$$\Phi_0 = \left(\frac{2d_0}{\beta_c}\right)[\cos((\beta_c)^{\frac{1}{2}}z) + 1], \tag{58}$$

where from (57c),

$$d_0 = d_0^- = d_0^+ = 0.321\,52. \tag{59}$$

This is simply the symmetric static solution to the Laplace–Young equation in (32) with $H_s = (2d_0/\beta_c)$ and zero contact angles. The quantity β_c is still undetermined from this leading-order matching but θ_0 can now be specified from (59) which stipulates that the leading-order curvatures of the inner asymptotes in regions II and III are identical

owing to matching with the symmetric outer solution with identical expansions at the two contact points $z_{\pm}$. For our initial condition with the fixed amplitude $\epsilon_0^- = 10^{-4}$, the asymptotic quadratic coefficient d_0^- in the $-y$-direction, unlike the universal $d_0^+ = 0.32152$ in the $+y$-direction, is a single-valued function of θ_0 only. Consequently, (59) allows us to determine θ_0 numerically to be

$$\theta_0 = -1.7206 \text{ radians}. \tag{60}$$

Without solving for Φ_1 explicitly, we first carry out the matching to yield

$$\Phi_1(z^{\pm}) = 0, \quad \Phi_1'(z^{\pm}) = \hat{b}_0^{\mp}, \tag{61a,b}$$

$$\frac{1}{2!}\Phi_1''(z^{\pm}) = 0, \quad \frac{1}{3!}\Phi_1'''(z^{\pm}) = \hat{e}_2^{\mp}, \tag{61c,d}$$

$$\frac{1}{4!}\Phi_1^{\mathrm{IV}}(z^{\pm}) = -\tfrac{1}{12}\beta_1 d_0, \quad \frac{1}{5!}\Phi_1^{\mathrm{V}}(z^{\pm}) = -\tfrac{1}{20}\beta_c \hat{e}_2^{\mp} = \tfrac{1}{120}\beta_c^2 \hat{b}_0^{\mp}, \tag{61e,f}$$

where the condition $H_1 = 0$ has been invoked. The only possible solution Φ_1 to (53*b*) that satisfies all the boundary conditions above is

$$\Phi_1 = 0. \tag{62}$$

This then immediately implies that

$$\beta_1 = 0 \tag{63}$$

and allows the determination of the two shifts $r^{\pm}$ from (61*b*) and (61*f*), which both stipulate $\hat{b}_0^{\mp}$ vanish exactly,

$$r^{\pm} = -b_0^{\pm}/2d_0. \tag{64}$$

This is equivalent to Bretherton's original insight that the matching should occur at the minimum of the asymptotic parabola in (49*a*), namely $\hat{b}_0^{\pm} = 0$, where the origin of the y-coordinate should lie. For $\epsilon_0^{\pm} = 10^{-4}$, the coordinate shifts are found to be $r^+ = 9.061$ and $r^- = -15.597$ with θ_0 given by (60). We have solved for θ_0, β_1 and $r^{\pm}$ and it remains to determine β_c, β_2 and β_3 (as well as $\epsilon_2^{\pm}$ from the inner equation and the 6 coefficients A_i, B_i and D_i ($i = 2$ and 3) from the Φ_2 and Φ_3 outer equations) from the matching conditions for Φ_2 and Φ_3.

The second-order outer equation (53*c*), unlike the leading-order equation (53*a*), is not symmetric with respect to $z \to -z$ and it accounts for the steepening of the front seen in the solitary waves. Its solution is

$$\begin{aligned}\Phi_2 = {} & A_2\cos((\beta_c)^{\frac{1}{2}}z) + B_2\sin((\beta_c)^{\frac{1}{2}}z) + D_2 \\ & + \cos((\beta_c)^{\frac{1}{2}}z)\left[\frac{\sin((\beta_c)^{\frac{1}{2}}z)}{\beta_c^{\frac{3}{2}}} + \frac{B_0\beta_2}{2(\beta_c)^{\frac{1}{2}}}z + \frac{A_0\beta_2}{4\beta_c}\cos(2(\beta_c)^{\frac{1}{2}}z) + \frac{B_0\beta_2}{4\beta_c}\sin(2(\beta_c)^{\frac{1}{2}}z)\right] \\ & + \sin((\beta_c)^{\frac{1}{2}}z)\left[-\frac{\cos((\beta_c)^{\frac{1}{2}}z)}{\beta_c^{\frac{3}{2}}} - \frac{A_0\beta_2}{2(\beta_c)^{\frac{1}{2}}}z + \frac{\beta_2 A_0}{4\beta_c}\sin(2(\beta_c)^{\frac{1}{2}}z) - \frac{B_0\beta_2}{4\beta_c}\cos(2(\beta_c)^{\frac{1}{2}}z)\right] \\ & - z/\beta_c - \beta_2\Phi_0(z)/\beta_c,\end{aligned} \tag{65}$$

and matching with H yields

$$\Phi_2(z^{\pm}) = \hat{a}_0^{\mp}, \quad \Phi_2'(z^{\pm}) = 0, \tag{66a,b}$$

$$\frac{1}{2!}\Phi_2''(z^{\pm}) = \hat{d}_2^{\mp}, \quad \frac{1}{3!}\Phi_2''(z^{\pm}) = \hat{e}_3^{\mp}, \tag{66c,d}$$

$$\frac{1}{4!}\Phi_2^{\mathrm{IV}}(z^{\pm}) = f, \quad \frac{1}{5!}\Phi_2^{\mathrm{V}}(z^{\pm}) = \tfrac{1}{120}\beta_c, \tag{66e,f}$$

where $$f = -\tfrac{1}{12}\beta_2 d_0 - \tfrac{1}{12}\beta_c(d_2^{\mp} - \tfrac{1}{2}\beta_c a_0^{\mp}) + \tfrac{1}{24}\beta_c^2 b_0^{\mp} r^{\mp} + \tfrac{1}{24}\beta_c^2 d_0^{\mp}(r^{\mp})^2. \tag{66g}$$

Expanding Φ_2 of (65) about the contact points $z_{\pm}$, (66) then become

$$-A_2 + D_2 - z_{\pm}/\beta_c - \frac{d_0\beta_2}{2\beta_c^2} = \hat{a}_0^{\mp}, \quad -\beta_c^{\frac{1}{2}}B_2 - \frac{1}{\beta_c} + d_0\beta_2 z_{\pm}/\beta_c = 0, \tag{67a,b}$$

$$\frac{1}{2!}\left(A_2\beta_c + \frac{d_0\beta_2}{2\beta_c}\right) = d_2^{\mp} - \tfrac{1}{2}\beta_c\hat{a}_0^{\mp}, \quad \frac{1}{3!}(B_2\beta_c^{\frac{3}{2}} - d_0\beta_2 z_{\pm}) = -\tfrac{1}{6}, \tag{67c,d}$$

$$\frac{1}{4!}(-A_2\beta_c^2 - \tfrac{5}{2}d_0\beta_2) = -\tfrac{1}{12}\beta_2 d_0 - \tfrac{1}{12}\beta_c(d_2^{\mp} - \tfrac{1}{2}\beta_c\hat{a}_0^{\mp}), \tag{67e}$$

$$\frac{1}{5!}(-B_2\beta_c^{\frac{5}{2}} + d_0\beta_c\beta_2 z_{\pm}) = \tfrac{1}{120}\beta_c. \tag{67f}$$

Subtracting the two versions of (67*a*) at the two contact points $z_{\pm}$ from each other yields our most important result

$$\beta_c = \left(\frac{2\pi}{\hat{a}_0^+ - \hat{a}_0^-}\right)^{\frac{2}{3}} = 1.413, \tag{68}$$

where the values of $\hat{a}_0^+ = 2.897$ and $\hat{a}_0^- = -0.842$ are obtained by integrating (38) with amplitudes $\epsilon_0^+ = \epsilon_0^- = 10^{-4}$ and θ_0 given by (60) in the initial conditions (39) and (41). (The shifts $r^{\pm}$, determined in the leading-order matching, are also involved.) This β_c can only be determined after using Φ_2 where mean-flow effects first appear.

Equations (67*c*) and (67*e*) are identical and equations (67*d*) and (67*f*) yield the same result. Subtracting the two versions of (67*d*) at the two contact points from each other yield

$$\beta_2 = 0. \tag{69}$$

Imposing this on (53*c*) for Φ_2, we conclude that, in contrast to the symmetric Φ_0, Φ_2 is not symmetric with respect to reflection in z. It still touches the contact points tangentially as seen in (66*b*) and hence, like Φ_0, yields a zero contact angle. However, from (66*a*), the two contact points are not equidistant from the fibre surface. (The vertical shift $\hat{a}_0^+$ is positive while $\hat{a}_0^-$ is negative and the absolute values are not identical.) The mean flow effect (+ 1 term in (53*c*)) is first felt at Φ_2 and it is Φ_2 that gives rise to the asymmetry of the coherent structures with a sloping back and a steep front. Since this asymmetry appears at δ^2, one expects the solitary waves to become increasingly symmetric as β approaches β_c.

The remaining equations are used to determine A_2, D_2, B_2 and $\epsilon_2^{\pm}$. They are given by

$$A_2 = 2d_2^+/\beta_c - \hat{a}_0^+, \quad B_2 = -\beta_c^{-\frac{3}{2}}, \quad D_2 = A_2 + \hat{a}_0^+ + z^+/\beta_c. \tag{70a–c}$$

The asymptotic coefficients of H_2 can now be determined. Like $\hat{a}_0^+$ and d_0^+, which are independent of ϵ_0^+, d_2^+ and $\hat{b}_2^+$ are independent of ϵ_2^+ provided ϵ_0^+ is fixed at the prescribed value of 10^{-4} and the corresponding r^+ shift is used. As ϵ_2^+ approaches zero, our numerical integration yields

$$2d_2^+ = 2.357, \quad \hat{b}_2^+ = -3.046, \tag{71a,b}$$

which will be used for front and higher-order matching. For the asymptote as $y \to -\infty$, (67*c*) implies that the initial amplitude ϵ_2^- in (46) must be chosen such that

$$2d_2^- = -2.926. \tag{72}$$

This is numerically found to be satisfied at

$$\epsilon_2^- = 5.0 \times 10^{-4}, \tag{73}$$

which also yields

$$\hat{b}_2^- = -8.148. \tag{74}$$

Since β_1 and β_2 vanish exactly, we must go to Φ_3 to determine how the solitary wave branch $c(\beta)$ decays from β_c. We shall only resolve Φ_3 near the contact points $z_\pm$ where Φ_0 vanishes. Near these points,

$$\Phi_3''' + \beta_c \Phi_3' = -\beta_3 \Phi_0', \tag{75}$$

with the solution

$$\begin{aligned}\Phi_3 \sim\ & A_3 \cos((\beta_c)^{\frac{1}{2}} z) + B_3 \sin((\beta_c)^{\frac{1}{2}} z) + D_3 \\ & + \cos((\beta_c)^{\frac{1}{2}} z)\left[\frac{\beta_3 A_0}{4\beta_c}\cos(2(\beta_c)^{\frac{1}{2}} z) + \frac{\beta_3 B_0}{4\beta_c}\sin(2(\beta_c)^{\frac{1}{2}} z) + \frac{\beta_3 B_0}{2(\beta_c)^{\frac{1}{2}}} z\right] \\ & + \sin((\beta_c)^{\frac{1}{2}} z)\left[-\frac{\beta_3 B_0}{4\beta_c}\cos(2(\beta_c)^{\frac{1}{2}} z) + \frac{\beta_3 A_0}{4\beta_c}\sin(2(\beta_c)^{\frac{1}{2}} z) - \frac{\beta_3 A_0}{2(\beta_c)^{\frac{1}{2}}} z\right] - \beta_3 \Phi_0(z)/\beta_c.\end{aligned} \tag{76}$$

Expanding Φ_3 in a Taylor series near $z_\pm$ provide a set of matching conditions like (57), (61) and (66). They allow solutions of β_3, A_3, B_3, D_3 and initial conditions for H_3 which are not necessary. Some of the matching conditions, such as the one corresponding to $\Phi_3(z_\pm)$, require the asymptotic behaviours of H_3. However, the contact angle condition which yields β_3 is matched only to H_2,

$$\Phi_3'(z_\pm) = \hat{b}_2^\mp. \tag{77}$$

From (71*b*) and (74), we see that Φ_3 provides the first non-trivial contact angles at the two contact points. More importantly, substitution of (76) into (77) yields

$$\tfrac{1}{2}\beta_3 A_0 z_\pm - B_3(\beta_c)^{\frac{1}{2}} = \hat{b}_2^\mp. \tag{78}$$

Subtracting the two equations in (78) as before, one obtains

$$\beta_3 = \beta_c^{\frac{3}{2}}(\hat{b}_2^- - \hat{b}_2^+)/2\pi d_0 = -4.242. \tag{79}$$

This then provides the leading non-trivial expansion of the solitary wave solution branch $c(\beta)$ near β_c,

$$c(\beta) \sim \frac{4.242}{1.413 - \beta}. \tag{80}$$

We have essentially carried out a matched asymptotic resolution of almost infinitely large homoclinic orbits.

We have also numerically traced the solitary wave solution branch. Our numerical scheme for the homoclinic orbit involves a numerical matching of the unstable manifold with a curve on the stable manifold. It is detailed in another application (Chang *et al.* 1993*a*) and we simply describe the results here. The constructed one-hump solitary wave solution branch is shown in figure 10 and it approaches infinity at $\beta_c = 1.41$, which is in excellent agreement with the predicted value in (68). This critical

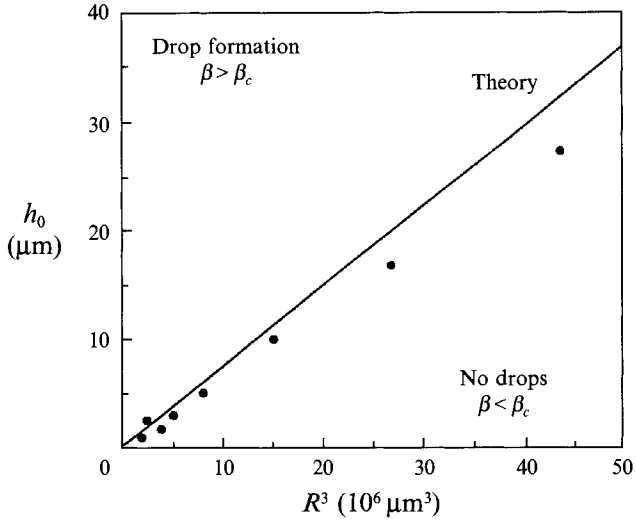

FIGURE 14. Comparison of the predicted $\beta_c = 1.413$ to the experimental data points (closed circles) of Quéré for the first formation of drops as the film thickness is increased.

β value clearly demarcates region with blow-up solutions from the saturated solutions. In figure 12, the numerically resolved speeds of the solitary waves are shown to approach the asymptotic expression of (80) near $\beta_c = 1.413$. Since it is difficult to numerically construct infinitely large solitary waves, the theoretical expression in (80) is probably more accurate. A particular member of the solitary wave branch at $\beta = 1.0$ is shown in figure 2 and is satisfactorily compared to the observed coherent structure. The slight difference in height is because the coherent structure is aligned in a periodic train and hence corresponds to a periodic solution near the homoclinic orbit generated by the Sil'nikov mechanism instead of being the actual homoclinic orbit. Nevertheless, the solitary wave is a good approximation of a coherent structure in the periodic train. Several constructed members of the solitary wave branch are shown in figure 13 with their phase-space trajectories. The rapid increase in the height of the solitary wave as β approaches β_c is evident. The decrease in the width of the outer region and in the wavelength of the bow waves and the increase in the decay rate of the bow waves with increasing β, predicted earlier, can also be seen.

Finally, the predicted $\beta_c = 1.413$ for the non-existence of the solitary wave branch corresponds to a critical film thickness of

$$h_c = 1.68 R^3 H^{-2} \tag{81}$$

from (8) and this is favourably compared to Quéré's experimental data for the formation of drops in figure 14. For $\beta > \beta_c$, solitary waves do not exist and drops are observed to form through the blow-up model while saturated waves are observed below β_c as the solitary-wave generated coherent structure prevents the blow-up phenomenon. The slight deviation at large R of our theory from the experimental data is because the lubrication approximation that leads to (7) is only valid if $h_0 \ll R$. Since h_c scales as $R^3 H^{-2}$, the theory begins to break down at $R \sim H$, that is when the fibre radius exceeds the capillary length H. As R approaches H, inertia becomes important as shown in §1 and contributes to the observed slight deviation.

5. Summary and conclusion

We have shown through numerical experiment that, after the linear inception region, all initial conditions below a critical β tend to approach an asymptotic interfacial dynamics dominated by solitary-wave-like coherent structures which do not involve amplitude growth of the wave crests. Above this critical β, amplitude growth of the wave crest continues and, in fact, accelerates after linear inception through a drastically different finite-time blow-up phenomenon dominated by a single ever-increasing static structure which eventually evolves into a drop on the fibre via other mechanisms. That the coherent structures created by mean-flow effects are generated by solitary waves allows us to estimate the critical β value by studying the existence of the solitary-wave solution branch. This solution branch approaches infinity at β_c and this allows an asymptotic determination of β_c via an expansion in $c^{-\frac{1}{3}}$. In fact, the argument that the solitary-wave-like coherent structure competes locally with the blow-up solution as attractors requires the solitary waves to be large. This may explain Pumir *et al.*'s observation of inertia-driven two-dimensional waves on a plane. The solitary-wave branch for that case exhibits a limit point at a critical parameter value with a finite-amplitude singular solitary wave. Below this critical value, both saturated dynamics and blow up are observed, depending on the initial condition. It is the infinitely large solitary waves at β near β_c in our case that is responsible for the clear demarcation for all initial conditions shown in figure 10. The two distinct behaviours of the solitary-wave solution branch are due to the dominant nonlinearities. In our case, the saturating axial curvature terms (triggered by the mean flow at one lower order), has exactly the same order of nonlinearity as the azimuthal curvature driven growth term. This allows balance between the two terms even at infinitely large amplitudes. In an inertia-driven flow, the stabilizing axial curvature term has a much lower nonlinear term than the destabilizing inertia term. As a result, for a finite Reynolds number, an infinitely large solitary wave is not possible and the absolute removal of the blow-up solution as an attractor by the coherent structures does not occur since the two leading-order structures are not identical. Consequently, both saturated waves and blow up are possible for the inertia-driven instabilities even when the solitary wave exists. As mentioned before, the latter phenomenon is likely to be eliminated by the introduction of transverse capillary effects and drop formation on an inertia-dominated film may never occur.

This work is supported by the Department of Energy through grant DE-FG02-92ER14269. We are grateful to Professor E. Demekhin and Mr. D. Kopelevich for their assistance in constructing the solitary waves in figure 13. We are also grateful to one of the reviewers for clarifying some details concerning the final evolution.

REFERENCES

AUL, R. W. & OLBRICHT, W. L. 1990 Stability of a thin annular film in pressure-driven, low Reynolds-number flow through a capillary. *J. Fluid Mech.* **215**, 585–599.

BRETHERTON, F. P. 1961 The motion of long bubbles in tubes. *J. Fluid Mech.* **10**, 166–188.

CHANG, H.-C. 1986 Traveling waves on fluid interfaces – normal form analysis of the Kuramoto–Sivashinsky equation. *Phys. Fluids* **29**, 3142–3147.

CHANG, H.-C. 1989 Onset of nonlinear waves on falling films. *Phys. Fluids* A **1**, 1314–1327.

CHANG, H.-C., DEMEKHIN, E. & KOPELEVICH, D. 1993*a* Laminarizing effects of dispersion in an active-dissipative nonlinear medium. *Physica* D **D63**, 299–320.

CHANG, H.-C., DEMEKHIN, E. & KOPELEVICH, D. 1993*b* Nonlinear evolution of waves on a vertically falling film. *J. Fluid Mech.* **250**, 433–480.

CHENG, M. & CHANG, H.-C. 1992 Stability of axisymmetric waves on liquid films flowing down a vertical column to azimuthal and streamwise disturbances. *Chem. Engng Commun.* **118**, 327–346.

ELPHICK, C., MERON, E. & SPIEGEL E. A. 1988 Spatiotemporal complexity in traveling patterns. *Phys. Rev. Lett.* **61**, 496–499.

FRENKEL, A. L. 1992 Nonlinear theory of strongly undulating thin films flowing down vertical cylinders. *Europhys. Lett.* **18**, 583–588.

FRENKEL, A. L., BABCHIN, A. J., LEVICH, B. G., SHLANG, T. & SIVASHINSKY G. I. 1987 Annular flows can keep unstable films from breakup: nonlinear saturation of capillary instability. *J. Colloid Interface Sci.* **115**, 225–233.

GLENDINNING, P. & SPARROW, C. 1984 Local and global behavior near homoclinic orbits. *J. Stat. Phys.* **35**, 645–696.

HAMMOND, P. S. 1983 Nonlinear adjustment of a thin annular film of viscous fluid surrounding a thread of another within a circular cylindrical pipe. *J. Fluid Mech.* **137**, 363–384.

KAWAHARA, T. & TOH, S. 1988 Pulse interaction in an unstable dissipative–dispersive nonlinear system. *Phys. Fluids* **31**, 2103–2111.

KERCHMAN, V. I. & FRENKEL, A. L. 1993 Interactions of coherent structures in a film flow: simulations of a highly nonlinear evolution equation. *Theoret. Comput. Fluid Dyn.* (to appear).

LIN, S. P. 1974 Finite-amplitude sideband instability of a viscous film. *J. Fluid Mech.* **63**, 417–429.

PARK, C.-W. & HOMSY, G. M. 1984 Two-phase displacement in Hele-Shaw cells: theory. *J. Fluid Mech.* **139**, 291–308.

PUMIR, A., MANNEVILLE, P. & POMEAU, Y. 1983 On solitary waves running down an inclined plane. *J. Fluid Mech.* **135**, 27–50.

QUÉRÉ, D. 1990 Thin films flowing on vertical fibers. *Europhys. Lett.* **13**, 721–726.

RATULOWSKI, J. & CHANG, H.-C. 1989 Transport of gas bubbles in capillaries. *Phys. Fluids* A **1**, 1642–1655.

ROSENAU, P., ORON, A. & HYMAN, J. M. 1992 Bounded and unbounded patterns of the Benney equation. *Phys. Fluids* A **4**, 1102–1104.

RUSSO, M. J. & STEEN, P. H. 1989 Shear stabilization of the capillary breakup of a cylindrical interface. *Phys. Fluids* A **1**, 1926–1937.

SCHWARTZ, L. W. 1989 Viscous flows down an inclined plane: instability and finger formation. *Phys. Fluids.* A **1**, 443–445.

SHLAG, T. & SIVASHINSKY, G. I. 1982 Irregular flow of a liquid film down a vertical column. *J. Phys. Paris* **43**, 459–466.

WILSON, S. D. R. 1982 The drag-out problem in film coating theory. *J. Engng Maths* **16**, 209–221.

WILSON, S. D. R. & JONES, A. F. 1983 The entry of a falling film into a pool and the air entrainment problem. *J. Fluid Mech.* **128**, 219–230.